


## Article

# Strengthening of Reinforced Concrete Structures with Carbon Reinforced Concrete—Possibilities and Challenges

Juliane Wagner <sup>1,\*</sup> , Carolin Würgau <sup>2</sup>, Alexander Schumann <sup>1</sup>, Elisabeth Schütze <sup>1</sup>, Daniel Ehlig <sup>2</sup>, Lutz Nietner <sup>2</sup> and Manfred Curbach <sup>3</sup>

<sup>1</sup> CARBOCON GMBH, Ammonstraße 72, 01067 Dresden, Germany; schumann@carbocon-gmbh.de (A.S.); schuetze@carbocon-gmbh.de (E.S.)

<sup>2</sup> Institut für Baustoffe und Bauverfahrensimulation, HTWK Leipzig, Karl-Liebknecht-Straße 132, 04277 Leipzig, Germany; carolin.wurgau@htwk-leipzig.de (C.W.); daniel.ehlig@htwk-leipzig.de (D.E.); lutz.nietner@htwk-leipzig.de (L.N.)

<sup>3</sup> Institut für Massivbau, TU Dresden, August-Bebel-Straße 30/30a, 01219 Dresden, Germany; manfred.curbach@tu-dresden.de

\* Correspondence: wagner@carbocon-gmbh.de

**Abstract:** The strengthening of existing reinforced concrete structures (RC) with carbon reinforced concrete (CRC) has a high potential to save resources and to increase the lifespan of the whole strengthened structure immensely. However, when strengthening structures with CRC, in some cases, failure due to concrete cover separation is detected, leading to the fact that the potential of the carbon reinforcement cannot be exploited. The prediction and prevention of this type of failure is the subject of current research. In this paper, a strut-and-tie-model is presented for calculating a critical tensile force leading to failure due to concrete cover separation. Additionally, possible methods to avoid that kind of failure are suggested. One of these is doweling the ends of the strengthening layer. This paper presents the first experiments to test this method, which show that doweling the strengthening layer leads to much higher failure loads compared to a structure without doweling. However, further investigations have to be examined to verify these first results.

**Keywords:** bending tests; carbon reinforced concrete; textile reinforced concrete; concrete cover separation; CRC; strengthening; carbon reinforcement; FRP



**Citation:** Wagner, J.; Würgau, C.; Schumann, A.; Schütze, E.; Ehlig, D.; Nietner, L.; Curbach, M. Strengthening of Reinforced Concrete Structures with Carbon Reinforced Concrete—Possibilities and Challenges. *CivilEng* **2022**, *3*, 400–426. <https://doi.org/10.3390/civileng3020024>

Academic Editor: Aires Camões

Received: 15 April 2022

Accepted: 10 May 2022

Published: 13 May 2022

**Publisher's Note:** MDPI stays neutral with regard to jurisdictional claims in published maps and institutional affiliations.



**Copyright:** © 2022 by the authors. Licensee MDPI, Basel, Switzerland. This article is an open access article distributed under the terms and conditions of the Creative Commons Attribution (CC BY) license (<https://creativecommons.org/licenses/by/4.0/>).

## 1. Introduction

The climate crisis is the main challenge of our time. To reduce the global CO<sub>2</sub> emission drastically, the building industry has to change! More than 50% of the CO<sub>2</sub> emissions can be traced back to the construction industry, e.g., [1]. One possible way to reduce the global CO<sub>2</sub> emission is to avoid demolition and preserve existing buildings by strengthening or retrofitting those structures. Very well-known and established methods for this include strengthening with shotcrete or CFRP-lamellas, -sheets, or -plates, e.g., [2–11]. Nevertheless, even when strengthening or retrofitting existing structures instead of demolishing them, we have to use more efficient and sustainable methods. One high potential method is carbon reinforced concrete (CRC) for strengthening or retrofitting existing reinforced concrete (RC) structures. The load-bearing-capacity of old concrete elements can be increased significantly, up to 300–400%, if they are strengthened with carbon reinforced concrete with a thickness of only 10 mm and just one layer of a carbon grid, e.g., [12]. Additionally, due to the high durability of the carbon fibers, the lifespan of the whole strengthened structure can be increased immensely.

Compared to conventional strengthening methods, e.g., the strengthening with shotcrete, up to 86% of resources and more than 50% of CO<sub>2</sub> emissions can be saved by using carbon reinforced concrete as a strengthening method, e.g., [13].

Carbon reinforced concrete has been investigated since ~1994 in Germany. Therefore, many research results and profound knowledge are already available. However, to implement the innovative strengthening method in the construction sector and to achieve an even more economical solution in a wider range of application, a few aspects have yet to be investigated.

In this paper, the state-of-the-art of strengthening with carbon reinforced concrete in Germany is shown. Moreover, the high potential of CRC is illustrated with a few practical examples which were or are executed right now in Germany. Lastly, current challenges and investigations concerning the safe load transfer between existing concrete members and carbon reinforced concrete will be presented. Moreover, experimental tests and a calculation model are presented for this case. Additionally, possible methods for solving this problem are shown.

## 2. Strengthening with Carbon Reinforced Concrete and Applicable Regulations

### 2.1. Carbon Reinforced Concrete as a Strengthening Method in a Nutshell

The innovative and high-performance material carbon reinforced concrete offers promising opportunities. With carbon reinforced concrete, sustainable and resource-saving constructions are possible not only in the area of new construction, but also for strengthening existing structures. This has already been demonstrated several times and described in the literature as well. For a general overview, see [12–27]. Especially in the field of renovation and strengthening of existing structures, carbon reinforced concrete has immense potential to strengthen and maintain structures and, thus, save them from demolition. Currently, too many structures are still being demolished although renovation and strengthening would be more efficient technically and economically. Demolition and new construction are often seen as the simpler choice. Above all, for ecological reasons the preservation of existing structures, as opposed to demolition and replacement, must be the top priority in planning and become the guiding principle of future building. This is the only way to create truly long-term sustainable constructions, to reduce emissions and save resources.

Carbon reinforced concrete is a composite material used for strengthening, consisting of a fine-grained concrete matrix and a carbon grid, arranged load-oriented in the concrete cross section. Compared to reinforcing with steel, carbon reinforcement is more corrosion-resistant and has up to six times the tensile strength. Thus, very thin strengthening thicknesses (usually 10 mm–20 mm) can be achieved (see Figure 1).

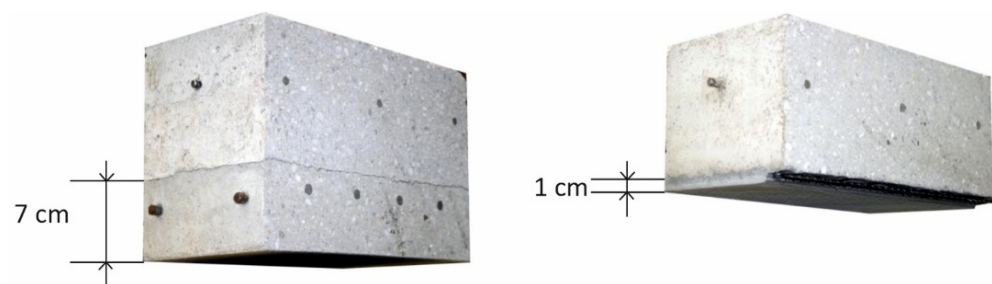


**Figure 1.** Comparison between the thickness of a shotcrete strengthening (**left**) and strengthening with carbon reinforced concrete (**right**) with the same load-bearing capacity. (Photo: TU Dresden).

As a result, compared to conventional shotcrete strengthening, resources and emissions can be saved when strengthening with specially developed fine-grained concrete combined with carbon reinforcement. The general structure and application of carbon reinforced concrete on the existing structures is based on the established process steps for shotcrete strengthening. The first layer of fine-grained concrete, which is in the range of 3–5 mm, is applied to the already prepared and sufficiently roughened old concrete surface by using either a spraying or a laminating method. The lightweight carbon grids are then applied onto the fresh concrete and the next layer of fine-grained concrete is sprayed on. This

process is repeated until the statically required number of layers is reached. After the application of the last layer of carbon grid, the final layer of fine-grained concrete is applied. As a final step, the surface of the concrete is cured accordingly.

The basic structure of an existing reinforced concrete element strengthened with carbon reinforced concrete is shown in Figure 2. In contrast to conventional shotcrete strengthening, strengthening with carbon reinforced concrete in a normal use, respectively if we are not in the field of bridge structures, does not require dowelling to affix the carbon grid to the existing concrete structure. A more efficient and economical method is therefore possible, and the existing structure is not damaged through dowelling afterwards. Another advantage in the field of renovation results from the very good bond behavior of the carbon grids and the resulting minimal crack widths in the concrete. The material is therefore ideally suited for restoration and increasing a structure's durability. As a result, the service life of building components and structures can be increased significantly.

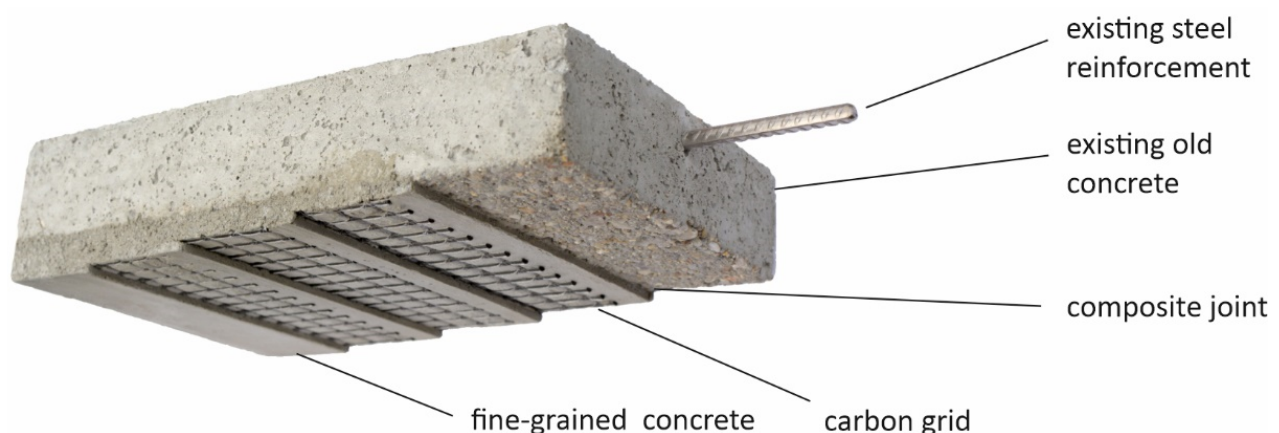


**Figure 2.** Exemplary structure of a strengthening with carbon reinforced concrete. (Photo: TU Dresden).

## 2.2. Applicable Regulations in Germany

Internationally there are already some regulations for the strengthening with CRC. Due to their large number, they will not be discussed in detail here. Instead, the authors deliberately focus on the regulations in Germany.

To date, there is no general regulation, standard or guideline for the use of CRC as a strengthening method in Germany. For the design of new concrete structures with non-metallic reinforcement, the first guideline by the German Committee for Structural Concrete (in German: Deutscher Ausschuss für Stahlbeton) will be published soon [28]. But this regulation is not valid for strengthening or retrofitting with CRC.

With the lack of regulations for new materials and technologies general technical approvals, general type approvals or general appraisal certificates are necessary. Those approvals or certificates regulate the application of new materials or techniques for all of Germany, but they are regulated for a restricted field of application only. If the planned design for a new building or a strengthening application differs from those restricted fields of application, individual approvals for the planned project are necessary. In Germany, there is one general building approval for the strengthening of existing structures with CRC, which will be described in the following section.

## 2.3. General Technical Approval for the Strengthening with Carbon Reinforced Concrete

### 2.3.1. General Overview

In 2014, after extensive theoretical and experimental preparatory work, the first general technical approval (in German: allgemeine bauaufsichtliche Zulassung "abZ") for the strengthening of reinforced concrete structures with textile reinforced concrete (TUDALIT; at first non-metallic reinforcement were called as textiles) was obtained by TU Dresden AG (TUDAG) from the German Institute for Building Technology (DIBt) [29]. An important

milestone for construction and strengthening with textile reinforced concrete had been reached. With this approval, textile reinforced concrete could be used in practice to a limited extent but in a regulated manner according to the building code. This means that valuable practical experience can be gained in the use of textile reinforced concrete and existing structures can be strengthened.

Carbon reinforced concrete, and in particular the properties of the material, have developed significantly since 2014. For example, current generations of carbon grids have almost twice the tensile strength (on average up to  $\sim 3500 \text{ N/mm}^2$ ) that grids of past generations had. Additionally, the bond between carbon grids and concrete as well as the temperature stability of the grids have been improved drastically. This is reflected positively in the design parameters. However, the normative basis for using the improved carbon grids for strengthening was missing in the general technical approval of 2014.

At the end of 2021 a new and extended approval for the strengthening of reinforced concrete structures with carbon reinforced concrete was granted by the DIBt [30]. Thereby, a regulated product with the designation CARBOrefit<sup>®</sup> is now available. The CARBOrefit<sup>®</sup> approval enables the safe, economical, and resource-saving use of carbon reinforced concrete in the area of strengthening and renovation.

To improve carbon reinforced concrete as a strengthening method in Germany a new and strong consortium was created. This consortium stands behind the CARBOrefit<sup>®</sup> approval. In particular, they want to work together to continuously develop the approval and therefore steer the construction industry towards sustainability.

The consortium consists of 11 highly qualified partners from the field of carbon reinforced concrete: four carbon grid manufacturers, two impregnation manufacturers, and one carbon fiber manufacturer. Moreover, the consortium involves one concrete manufacturer, one forming manufacturer, one engineering (planning) company, and the project leader/coordinator, CARBOCON GMBH:

1. CARBOCON GMBH;
2. cbing—Curbach Bösche Ingenieurpartner;
3. CHT Germany GmbH;
4. Hitexbau GmbH;
5. Johne & Groß GmbH;
6. PAGEL Spezial-Beton GmbH & Co. KG;
7. Solidian GmbH;
8. Teijin Carbon Europe GmbH;
9. TUDATEX GmbH;
10. Wilhelm Kneitz Solution in Textile GmbH;
11. Zschimmer & Schwarz Chemie GmbH.

### 2.3.2. Materials

The CARBOrefit<sup>®</sup>-fine-grained concrete (TF10-PAGEL by PAGEL Spezial-Beton GmbH & Co. KG, Essen, Germany) is used in the new approval for the strengthening of steel reinforced concrete structures with carbon reinforced concrete. It is produced as a dry mortar consisting of cement, silicate dust, fly ash, and quartz sand with a maximum grain size of 1 mm and has the material properties listed in Table 1.

**Table 1.** Characteristics of the CARBOrefit<sup>®</sup> fine-grained concrete, according to [30].

Characteristics	Unit	Value
Compressive strength (characteristic value after 28 days) <sup>1</sup>	[N/mm <sup>2</sup> ]	≥80
Flexural tensile strength (characteristic value after 28 days) <sup>1</sup>	[N/mm <sup>2</sup> ]	≥6
E-modulus (mean value after 28 days)	[N/mm <sup>2</sup> ]	≥25,000

<sup>1</sup> Tested with mortar prisms  $40 \times 40 \times 160 \text{ mm}^3$  according to DIN EN 169-1 [31].

High-performance carbon grids are used as reinforcements in the strengthening system. The carbon grids are composite materials made of carbon fibers and a polymer



impregnation. The carbon fibers and the impregnation are combined to form the carbon grids. Various carbon grids are available in the new CARBOrefit® approval for the strengthening of existing steel reinforced concrete structures, which can be selected depending on the degree of strengthening required and the application.

The standard design of the carbon grid defined in the approval has the geometry shown in Figure 3 on the left. It has a cross-sectional area of  $140 \text{ mm}^2/\text{m}$  in warp direction. In addition to this standard version, the geometric properties can be configured individually (e. g. Figure 3, right). In Table 2, the possible geometries according to the approval are shown. Through this, the carbon grid can be optimized with regard to the circumstances of the specific construction project and the resulting boundary conditions. In doing so, a significant cross-section of the reinforcement can be saved in applications with less cross-section necessary. Therefore, a more economical solution is possible. In Table 2, the limits of the different carbon geometries are listed.

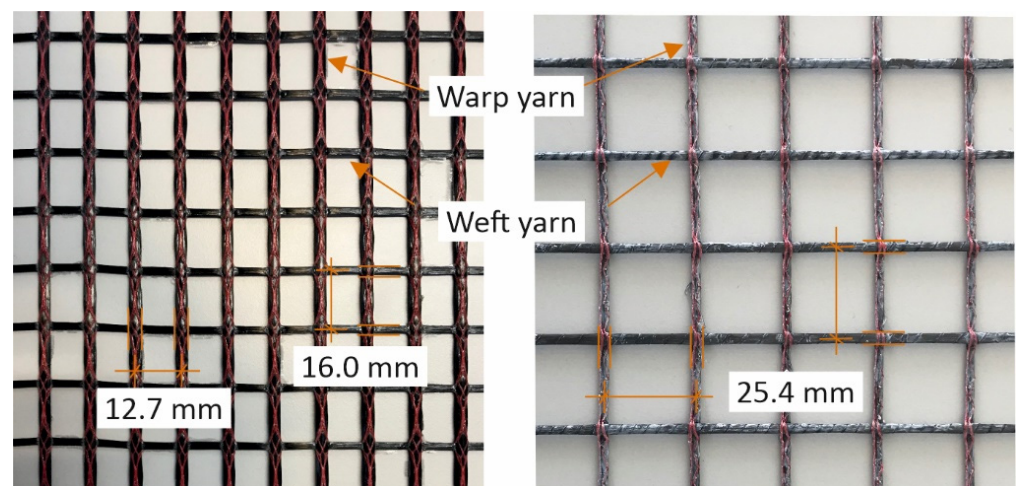


**Figure 3.** Possible carbon grid geometries. (Photo: CARBOCON GMBH).

**Table 2.** Permitted range of geometric properties of the CARBOrefit®-grid standard design and special design, according to [30].

Version	Property	Unit	Warp Yarn	Weft Yarn
Standard	Fiber content	[K]	$\geq 48$ and $\leq 50$	12
	Cross-sectional area of the yarns	$[\text{mm}^2]$	$\geq 1.8$ and $\leq 1.95$	0.45
	Yarn spacing	[mm]	12.7	$16 +0/-2$
Special	Fiber content	[K]	$\geq 48$ and $\leq 50$	$\geq 12$ and $\leq 50$
	Cross-sectional area of the yarns	$[\text{mm}^2]$	$\geq 1.8$ and $\leq 1.95$	$\geq 0.45$ and $\leq 1.95$
	Yarn spacing	[mm]	$\geq 12.7$ and $\leq 50.8$	$\geq 16 +0/-2$ and smaller than twice the yarn distance in warp direction
	Additional requirements	[-]		$\geq 20\%$ of the cross-sectional area in warp direction

In addition to the variation of the geometric properties of the carbon grids, the approval allows the selection between different types of yarns. These yarns differ in their mechanical properties (e.g., tensile strength, bond behavior, and flexibility of the carbon grid), which is caused by the use of different impregnations. In Table 3, the mechanical properties of the different carbon yarns are shown in detail.

**Table 3.** Mechanical properties of the different CARBOrefit®-grids, according to [30].

Property	Unit	Type 1	Type 3
Characteristic tensile strength	[N/mm <sup>2</sup> ]	1550	2250
Design tensile strength	[N/mm <sup>2</sup> ]	768	1300
E-modulus	[N/mm <sup>2</sup> ]	206,667	206,667
Max. strengthening force	[kN/m]	430	430
Design bond strength	[N/mm]	0.564	4.7
Anchoring length	[mm]	2450	500
Flexibility	[-]	very bendable	less bendable

In Table 3, the design strengths of the different types are listed. For the evaluation of the different design values, the reduction factors behind the design values must be mentioned. These take into account the mechanical behavior and the reductions of the types with regard to various exposures, such as the temperature, long-term exposure, durability, etc.

Here, the significant improvement in the mechanical properties of the yarn type 3 under long-term load, temperature exposure (40 °C), and its durability against chemical exposure can be highlighted. As can be seen in Table 4, the reduction factors of the carbon grid, taking into account the material properties for both the tensile strength and the bond strength, were significantly improved compared to the carbon yarn type 1 and compared to previous carbon grids. The high performance of the new carbon grids can be taken into account in the design now, which will lead to a more economical design of the strengthening system.

**Table 4.** Reduction coefficients for temperature exposure (40 °C), continuous exposure and chemical exposure, according to [30].

Reduction Factors	Type 1	Type 3
<b>Tensile strength</b>		
Temperature influence (40 °C)	0.85	1.00
Long term load	0.70	0.70
Durability	1.00	1.00
<b>Bond strength</b>		
Temperature influence (40 °C)	0.45	1.00
Long term load	0.47	0.70
Durability	1.00	1.00

### 2.3.3. Scope of the CARBOrefit® Approval

The CARBOrefit® approval opens up new possibilities for planners when designing solutions. Now, planners can select different types of carbon grids that optimally match the existing structure in terms of mechanical properties and geometry.

Nowadays, the scope of the CARBOrefit® approval includes the uniaxial flexural strengthening of the tension zone of steel reinforced concrete elements, which do not require shear reinforcement. The reinforcement may also be placed in the compression zone, but the carbon grid mustn't transfer any forces. Several layers of carbon grids can be used to strengthen the tension zone. The number of carbon grid layers depends primarily on the load-deficit and the type of the used carbon grid. Furthermore, strengthening is currently limited to interior structures under predominantly static loads that do not exceed a maximum temperature of 40 °C and a relative humidity of 65%. The components to be strengthened must have an adhesive strength of at least 1.0 N/mm<sup>2</sup> (statistical evaluation according to [28]) and the properties of the old concrete must be in the range of a concrete of strength class <C50/60. In addition, the concrete cover of the existing steel reinforcement must be ≥10 mm.

The limited area of application is to be continuously expanded so that in the future many structures can be strengthened with CRC on the basis of the approval. A large number of practical examples shows the possibilities of carbon reinforced concrete as a strengthening method. Some practical examples are presented in the following chapter.

### 3. Practical Applications

#### 3.1. General Overview

The benefits and opportunities of the carbon reinforced concrete strengthening system have been proven in a number of practical applications. Starting from early projects, such as the strengthening of a saddle roof in Schweinfurt in 2006 and a barrel roof in Zwickau in 2008 (e.g., [32]), the applicability of the strengthening process has evolved to include a wide variety of structures. Applications for strengthening and retrofitting with carbon reinforced concrete include but are not limited to a number of silos, bridges, and more [33–40]. In the following sections, a few projects with a CRC strengthening will be shown. All of them were realized outside the scope of the approval presented in Section 2 of this paper. Therefore, for each of them, individual approval was necessary.

#### 3.2. Strengthening of the Hypar Shell in Magdeburg

Built in 1969 according to the plans of civil engineer Ulrich Mütter, the hypar shell in Magdeburg is one of the largest concrete shell structures of its kind. The steel reinforced concrete roof construction consists of four hyperbolic paraboloid shells. In total, the 7 cm thin concrete shell has a span of 48 m × 48 m without any supports.

The first structural damages to the hypar shell occurred shortly after completion. Over the years, the damage increased, and it became necessary to search for a suitable strengthening concept. At first, it was planned to strengthen the hypar shell with conventional methods, e. g. strengthening with steel reinforced shotcrete. To strengthen the thin concrete shell with shotcrete, two layers of 7 cm each, one on top and one on the bottom of the concrete shell, were planned (Figure 4). However, the existing structure would not have been able to bear the additional dead load (from 7 cm up to 21 cm). Therefore, initially no suitable conventional strengthening method was found. Based on an as-built analysis, it was decided to strengthen the shell construction with a 10 mm thin carbon reinforced concrete layer including one layer of carbon grid each on the top and on the bottom of the shell structure.

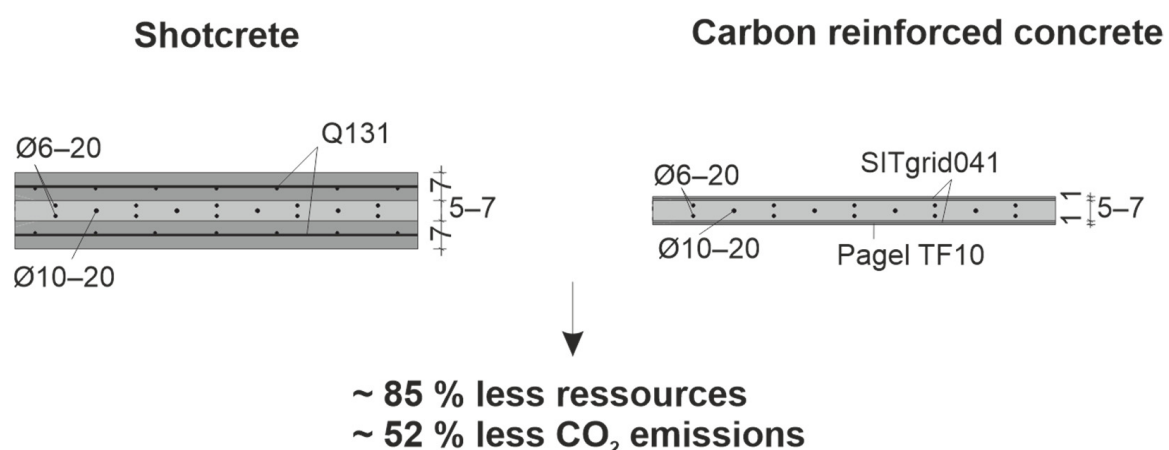


**Figure 4.** Comparison of strengthening with shotcrete or CRC. (Graphic: CARBOCON GMBH).

By using carbon reinforced concrete, the unique structure was saved from demolition. The strengthening works were carried out between February 2020 and July 2021 (Figure 5). For more information, see [41–43].





**Figure 5.** Strengthening process of the hypar shell in Magdeburg with CRC from 2020. (Photo: M. Bredt).

### 3.3. Strengthening of the Beyer Bau in Dresden

The Beyer Bau building complex located on the TU Dresden campus was constructed between 1910 and 1913 (Figure 6). The main structure, including the floors and parts of the roof, are made of steel reinforced concrete. Thus, the Beyer Bau is one of the first steel reinforced concrete buildings in Dresden.



**Figure 6.** View of the Beyer Bau. (Photo: S. Gröschel).

With an age of over 100 years, the Beyer Bau needs to be renovated today. As part of the renovation, structural deficits of ceiling slabs and beams are to be compensated by using carbon reinforced concrete. The deficits are mostly the result of increased utilization requirements and a very slender existing construction. The beams are strengthened with two layers of carbon grid. Thus, the thickness of the strengthening layer is 15 mm. For

strengthening the ceiling slabs, one layer of carbon grid is used. Therefore, the thickness of the CRC layer is 10 mm.

For receiving the individual approval among other tests, large-scale component tests were necessary in order to be able to demonstrate the suitability of the strengthening system even on beams and a concrete with very low strength (C8/10). This was achieved through tests on four large components (Figure 7) reflecting the realities of the existing system in all relevant points. The tests proved that, even with very low concrete strengths and smooth steel reinforcement with large diameters, a significant increase in the load bearing capacity is possible with a strengthening layer with a thickness of only 1–1.5 cm and a maximum of two layers of carbon grid. Therefore, the unique structure was saved from demolition.



**Figure 7.** Large-scale component test during the individual approval process. (Photo: CARBOCON GMBH).

The strengthening work of the Beyer Bau has started in July 2021.

### *3.4. Strengthening of a Pedestrian Bridge in Naumburg*

The historical arch bridge Thainburg in Naumburg is one of the oldest, still preserved reinforced concrete bridges in Germany (Figure 8a). The bridge, which is listed as a historic monument, was built in 1893. Over the last few decades, corrosion damage has occurred in the structure, so that a renovation concept became necessary. For material efficiency and aesthetic reasons, the innovative strengthening with carbon reinforced concrete was chosen. The strengthening layer thickness is only between 6 and 9 mm. The carbon grids were applied in one and two layers.

The reinforcement work was carried out between July and September 2021. The use of the extremely thin carbon reinforced concrete strengthening made it possible to meet the requirements for monument protection in Germany (Figure 8b).





(a)



(b)

**Figure 8.** View of the historical arch bridge Thainburg: (a) before strengthening; (b) after the strengthening with carbon reinforced concrete. (Photos: CARBOCON GMBH).

### 3.5. Strengthening of the First Motorway Bridge in Germany

The 70 m long bridge of the A648 motorway crosses two cycle paths and the river Nidda near Frankfurt (Figure 9). The three-span prestressed concrete bridge was built in 1971. In order to increase the lifespan of the construction, it was strengthened with carbon reinforced concrete between 2020 and 2021. This was the first time that carbon reinforced concrete was used to strengthen a motorway bridge. Five layers of carbon reinforcement were used on the top and six layers on the bottom side. Therefore, the reinforcement layer thickness is up to 35 mm on both sides. For more information, see [44–46].



**Figure 9.** View of the motorway bridge over the river Nidda. (Photo: Oliver Steinbock).

## 4. Current Challenges in Research

### 4.1. Strengthening with Carbon Reinforced Concrete—Challenges

Reinforced concrete members strengthened with carbon reinforced concrete can show a number of failure mechanisms that have to be considered in the dimensioning of strengthening layers for flexural strengthening. Figure 10 summarizes common failure modes. Design usually primarily aims at preventing tensile rupture of the reinforcement, while

also avoiding failure of the concrete in the compression zone. In addition to that, the carbon reinforcement must be anchored sufficiently. As the strengthening layer can usually only be applied in the clear span of flexural members up to the supporting structure, reinforcement cannot be anchored beyond the supporting structure, resulting in limited anchorage length for the carbon reinforcement. Comparatively high tensile stresses in the carbon reinforcement often have to be transferred into the concrete on a short length. This can lead to a number of challenges. To enable the transfer of high loads on a short anchorage length bond strength has to be high enough to avoid pull-out failure. In addition, the tensile strength of the concrete around the reinforcement has to be sufficiently high to prevent spalling of the concrete cover caused by high bond stresses. Both can be attained using state-of-the-art high-performance materials (like the CARBOrefit®-materials described in Section 2.3.2) for both reinforcement and concrete in the strengthening layer.

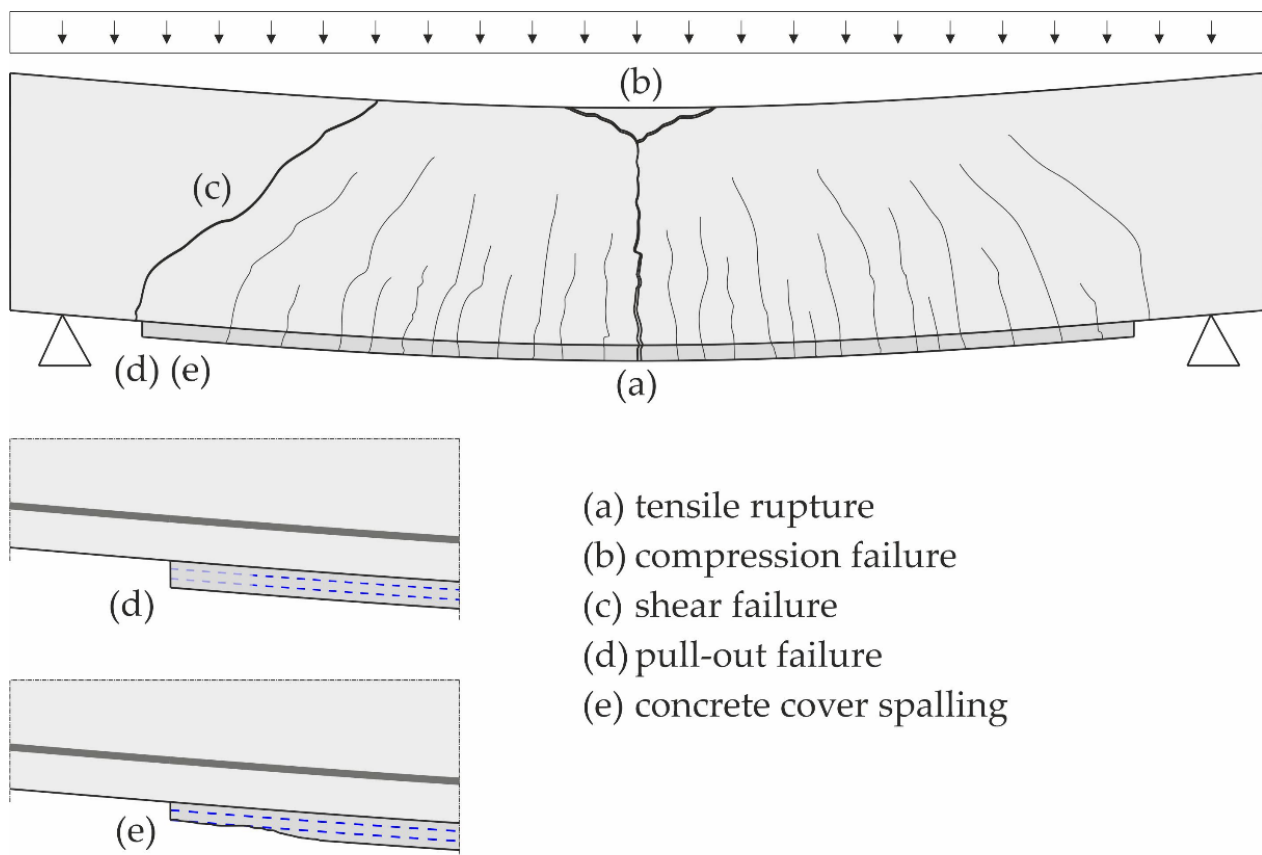


**Figure 10.** Common failure modes in reinforced concrete members strengthened with carbon reinforced concrete. (Graphic: CARBOCON GMBH).

However, in some cases strengthening with CRC presents itself with challenges beyond that. When high loads have to be transferred on a short length, not only the strengthening layer, but also the reinforced concrete member itself and the joint between both must be able to withstand the resulting forces. This was found to be a challenge in some projects and practical applications, where a high number of high-strength carbon reinforcement layers was applied, the available anchorage length was relatively short, or the reinforced concrete member showed very low concrete strength. Especially in configurations that meet a combination of these conditions, premature failure of CRC-strengthened RC-members was detected, although neither tensile failure of the reinforcement, compression failure of the concrete nor failure of the bond between reinforcement and concrete could be detected. Instead, the critical failure mode was found to be a detachment of the strengthening layer, a failure mode that is common in strengthening with FRP-sheets (see [47]) but has only

recently occurred in strengthening with carbon reinforced concrete. It is caused by the detaching tensile stress resulting from high loads having to be transferred between RC-member and CRC-strengthening layer locally exceeding the transverse tensile strength of either RC-member, bonding zone or reinforcement layer. Figure 11 shows a selection of forms in which the bonding area between RC-member and strengthening layer can fail.

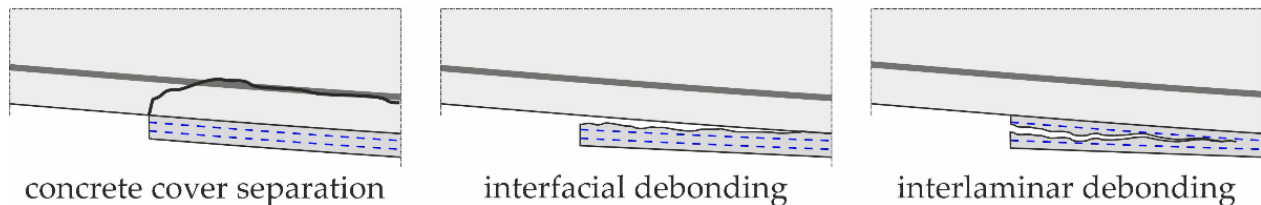


**Figure 11.** Failure modes in the bonding area of RC beams strengthened with carbon reinforced concrete. (Graphic: CARBOCON GMBH).

One such failure mode was detected in a project, where up to 6 layers of high-strength carbon reinforcement were to be fully anchored on a length of 61 cm at maximum. In bending tests on RC-beams strengthened with up to six layers of carbon reinforcement (see Figure 12), that were conducted to verify the design of the strengthening layer, the tension of the carbon reinforcement peaked at only 60% of the design strength before the beam failed due to concrete cover separation at the end of the strengthening layer; see Figure 13. Due to the short length available for force transmission, forces could not be transmitted sufficiently into the RC-beam.

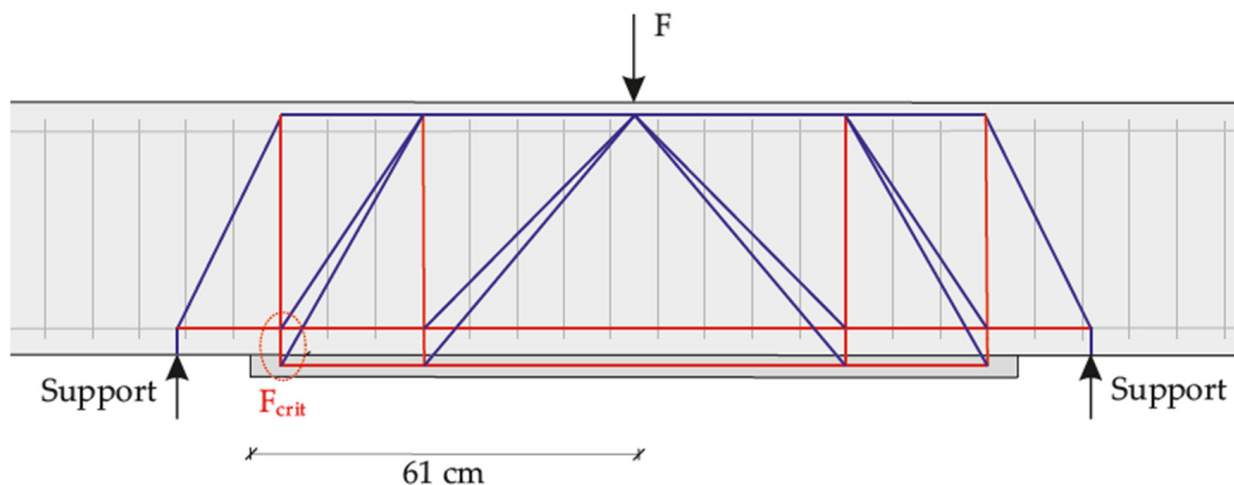


**Figure 12.** Strut-and-tie-model for the calculation of the critical tensile force, that induced concrete cover separation. (Graphic: CARBOCON GMBH).

To understand and quantify the premature failure of the beam, a strut-and-tie-model was conceived. This served to determine the tensile forces in the bonding area, which could then be compared to the strength of the bonding area. Conditions for the design of the strut-and-tie-model were derived from the positioning of the reinforcement in the test specimens and the failure observed in the tests: As the debonding started at the end of the strengthening layer, it was concluded that the critical vertical tensile strut  $F_{crit}$  representing the tensile forces in the bonding area must have formed close to the end of the strengthening layer. It was also assumed, that the vertical tensile struts generally orientate towards the stirrups that constitute the shear reinforcement. Based on this, the critical tensile strut was arranged at the first stirrup in the strengthened area. The inclination of the compression struts was derived from the crack pattern of the specimens. The resulting strut-and-tie-model is shown in Figure 12.



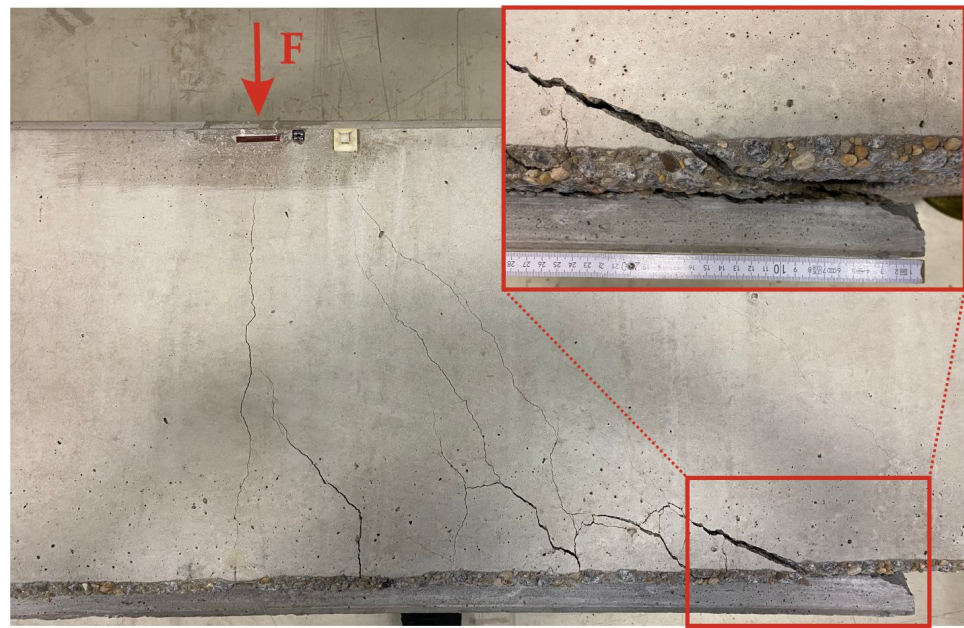


**Figure 13.** Concrete cover separation at the end of the strengthening layer with 6 layers of carbon reinforcement. (Photo: CARBOCON GMBH).

The resistance force of the bonding area was calculated from the tensile strength of the concrete in the RC-member and the area the critical tensile force  $F_{crit}$  acts on, which equates to the bonding area between RC-member and strengthening layer, limited to the end of the strengthening layer at one end and the first flexural crack in the strengthened area at the other end.

For the test shown in Figure 12, the critical tensile force  $F_{crit}$  calculated by setting the acting force  $F$  to the failure load from the tests equaled the resistance force with a deviation of only 4%. Thus, the established strut-and-tie-model was shown to be able to reproduce the failure mode observed in this test. However, to not only comprehend the failure observed in the tests, but also solve the problem of premature failure due to concrete cover separation, methods to enhance the resistance force of the bonding area must be found: For the strengthened beam shown here, a calculation based on the same strut-and-tie-model shows, that the resistance force of the bonding area would have to be more than doubled, to be able to transfer the force resulting from reaching the characteristic tensile strength of the carbon reinforcement. Therefore, the authors considered possible solutions for increasing the resistance force of the bonding area. The most promising of them are presented in the following section.

#### 4.2. Possible Solutions to Avoid Concrete Cover Separation

The basis of all solutions presented below is the strut-and-tie-model shown in Figure 12. All methods either aim to increase the resistance force of the bonding area or to reduce the critical tensile force  $F_{crit}$ .

Therefore, a first possible solution for avoiding concrete cover separation is staggering the ends of the carbon grid layers within the strengthening layer (Figure 14a). With this arrangement, the risk of failure caused by concrete cover separation might be reduced, since the tensile force in the CRC layer is gradually introduced into the concrete beam due to the staggered ends.

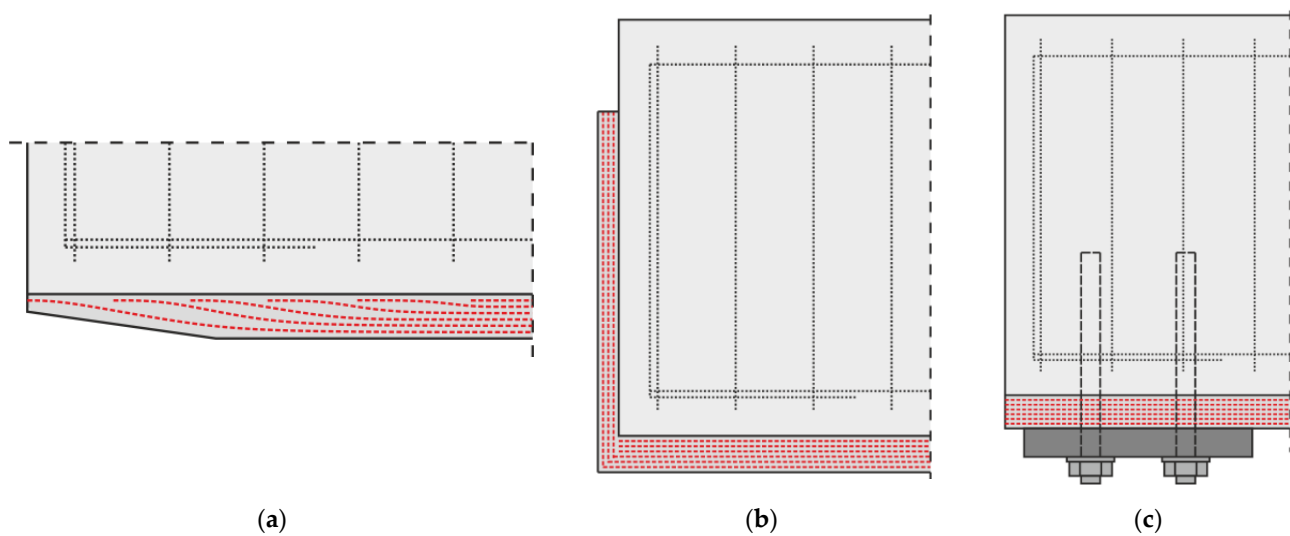


**Figure 14.** Possible solutions to avoid concrete cover separation: (a) staggered carbon reinforcement; (b) leading carbon reinforcement upwards behind the support; (c) doweling. (Graphic: CARBOCON GMBH).

The second option is to bend the carbon grid layers upwards at the end of the beam behind the supports (Figure 14b). As a result, the forces are introduced laterally into the component instead of being introduced at the bottom, which would support the separation of the concrete cover. The anchoring can be either made out of a prefabricated angle out of carbon reinforcement which overlaps the carbon reinforcement at the bottom of the beam. Another possibility is to bend the carbon reinforcement upwards from the bottom layer itself. One disadvantage of this solution is that bending the carbon reinforcement behind the support is not possible in every type of structure.

The third option is the use of additional dowels (Figure 14c). The dowels should be arranged around the critical tensile strut from the strut-and-tie-model and introduce the tensile loads into the concrete beam.

The effectiveness of all three methods has to be examined in several tests. First investigations considering the method of doweling the ends of the strengthening layer have already been carried out. The aim of the investigations was to check in general if the use of dowels increases the load at which failure occurs, to verify the assumed strut-and-tie-model and to measure the forces in the critical tensile strut. The investigations are presented in the following section.

## 5. Experimental Investigations

### 5.1. Materials and Methods

#### 5.1.1. Specimen—Geometry and Material

In these investigations, two reinforced concrete beams with a strengthening layer of CRC were tested: one as a reference test without dowels (specimen 1) and a second one with doweled ends of the strengthening layer (specimen 2); see also Table 5.

**Table 5.** Overview of the tested specimen.

Specimen	Doweling of the Strengthening Layer?	Sample Number
1	no	1
2	yes	1

The specimen geometry replicated the strengthened RC-beam in which concrete cover separation first occurred (see Section 4.1): The two reinforced concrete beams were 270 cm long, 50 cm wide and 40 cm high and had a predetermined breaking point right in the middle of their length. The strengthening layers were 122 cm long (which equals



an anchoring length of 61 cm in both directions from the predetermined breaking point), 32 cm wide and 3.5 cm high. The RC beams were made out of concrete C45/55. The lower and upper longitudinal reinforcement of the beams consisted of 5Ø12 each. Additionally, a stirrup reinforcement of Ø12 every 7.5 cm was arranged to avoid shear failure of the beams. Figure 15 shows the dimensions of the specimens and their reinforcement.

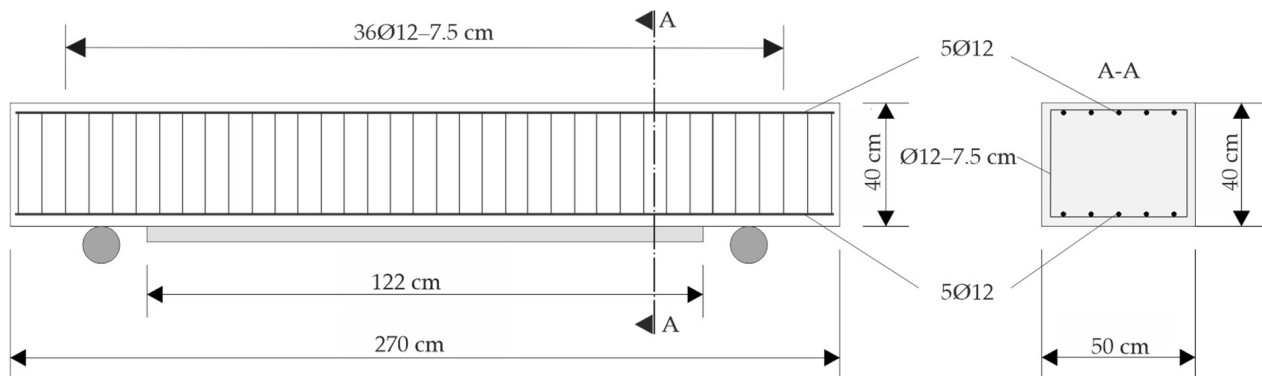


**Figure 15.** Dimensions of the specimens and their reinforcement. (Graphic: CARBOCON GMBH).

The RC beams were strengthened with 6 layers of CRC each. The used carbon grid corresponded to the standard design of CARBOrefit®-grid type 3 from Section 2.3.2 of this paper. Only the used impregnation of the carbon fibers differed from the one used in the CARBOrefit® approval. For the experiments presented, a polyacrylate impregnation was used. However, the mechanical properties of the carbon grids presented in Section 2.3.2. remain the same. The carbon grids were embedded in the CARBOrefit® fine-grained concrete described in Section 2.3.2.

As mentioned before, one of the reinforced concrete beams was tested with doweled ends of the strengthening layer. For this, steel dowels Würth Fixanker with a diameter of 24 mm and a length of 220 mm were used. Further information about the dowels can be found in [48]. However, there is no indication of the magnitude of E-modulus in this approval.

### 5.1.2. Manufacturing of the Specimen

During the manufacturing of the RC-beams, their bottom surface was produced as washed concrete for receiving a roughened surface for the application of the strengthening layer according to the requirements of the CARBOrefit® approval [30]. After 14 days, the strengthening layer was applied in a lamination process. In order to ensure that the carbon layers were exactly aligned, two position holders were used. When the specimens were tested, they were approximately 500 days old. As mentioned before, one beam was tested as a reference test without dowels (specimen 1) and the other beam was tested with doweled ends of the strengthening layer (specimen 2). For this, four dowels were set on each side. They were prestressed by applying a tightening torque of 200 Nm. Each dowel group was supposed to be placed in such a way that their resulting force matches the location of the assumed critical tensile strut. However, inserting the dowels did not work as expected, so the dowels were located offset to the critical tensile strut. The planned and final location of the dowels are shown in Figure 16.

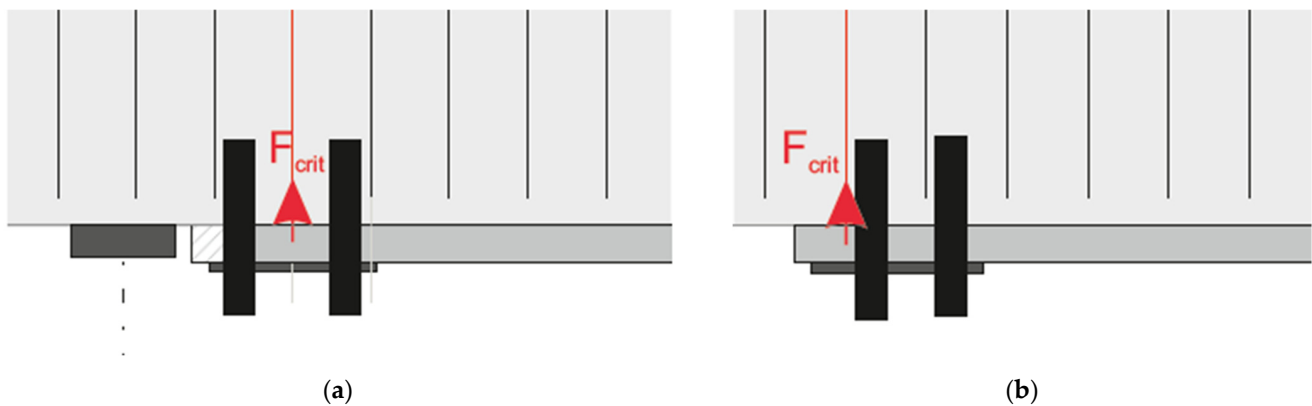


**Figure 16.** Location of the dowels: (a) planned location; (b) final location. (Graphic: CARBOCON GMBH).

### 5.1.3. Test Setup and Measuring Technology

The tests were carried out as 3-point bending tests at HTWK Leipzig. The specimens were supported fixed on one and moveable on the other end with a distance of 145 cm between supports. Behind the supports, the beam protruded approximately 62.5 cm on each side to ensure a proper anchoring of the steel reinforcement. The load was introduced at the top center of the beam via a 4 cm wide steel profile, which was mounted on a very stiff rubber plate, as shown in Figure 17.

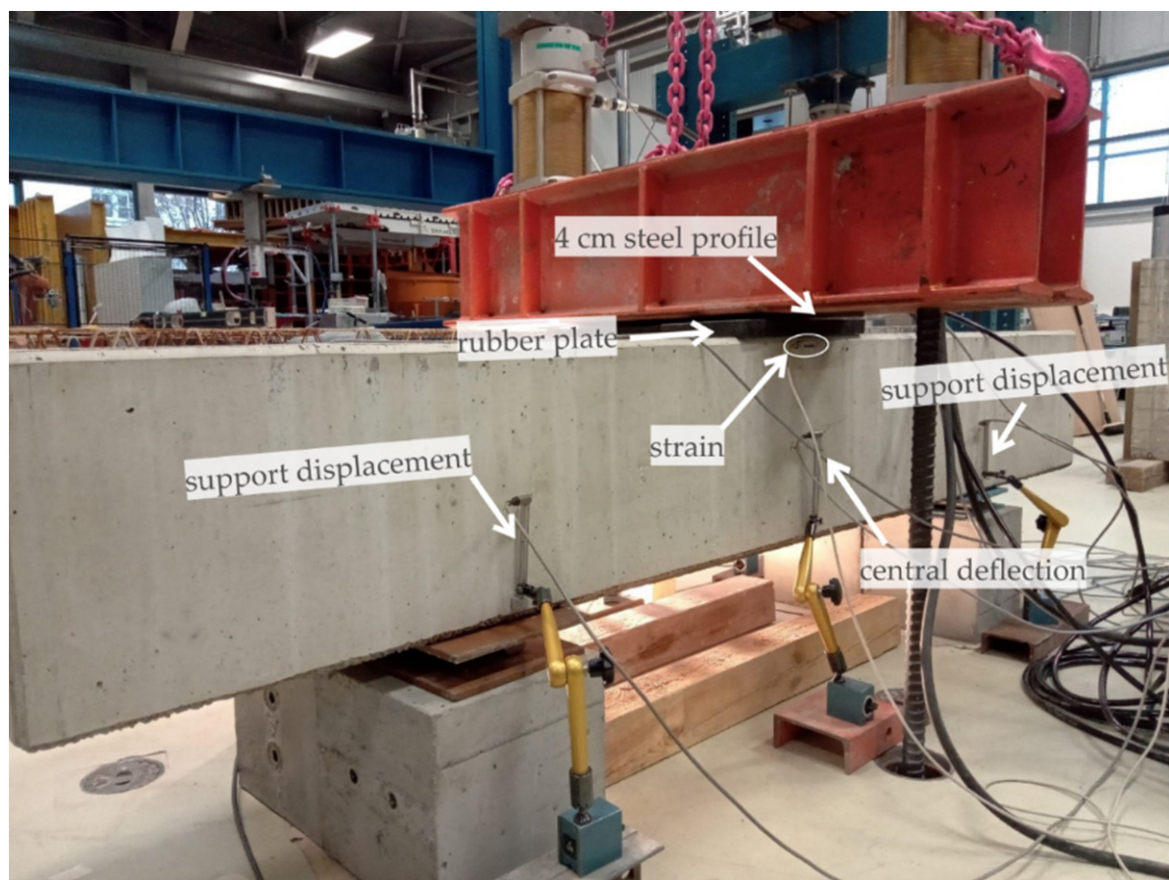


**Figure 17.** Test setup of the experimental investigations. (Photo: HTWK Leipzig/CARBOCON GMBH).

The following values were measured:

- vertical support displacement;
- central deflection;

- strain at the top of the beam in the area of load introduction;
- applied load.

Additionally, the following values were measured on specimen 2:

- strain at the bottom center of the strengthening layer;
- strain inside two of the four dowels on each side, as shown in Figure 18.



Bottom view of specimen 2:

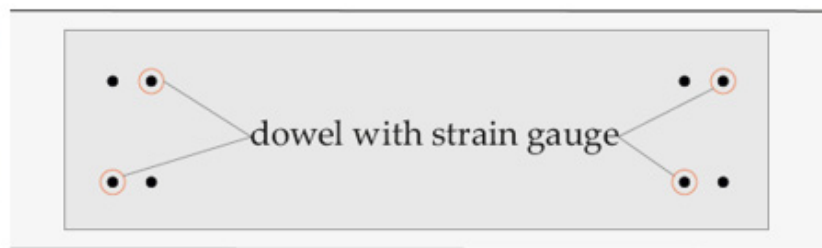


**Figure 18.** Anchor bolts with strain gauge. (Photo: HTWK Leipzig).

#### 5.1.4. Load Regime and Experimental Program

For the 3-point bending tests, first a preload of 50 kN was applied to the beams to check the centering of the load introduction. Afterwards, the specimens were loaded with a hand pump with a loading speed of approximately 0.15 mm/min. In defined intervals, the loading was stopped for about 90 s to check the beam for new cracks and measure the crack widths. In Figure 19, the planned applied load, the associated calculated stress of the carbon grids and the points of stopping are shown.

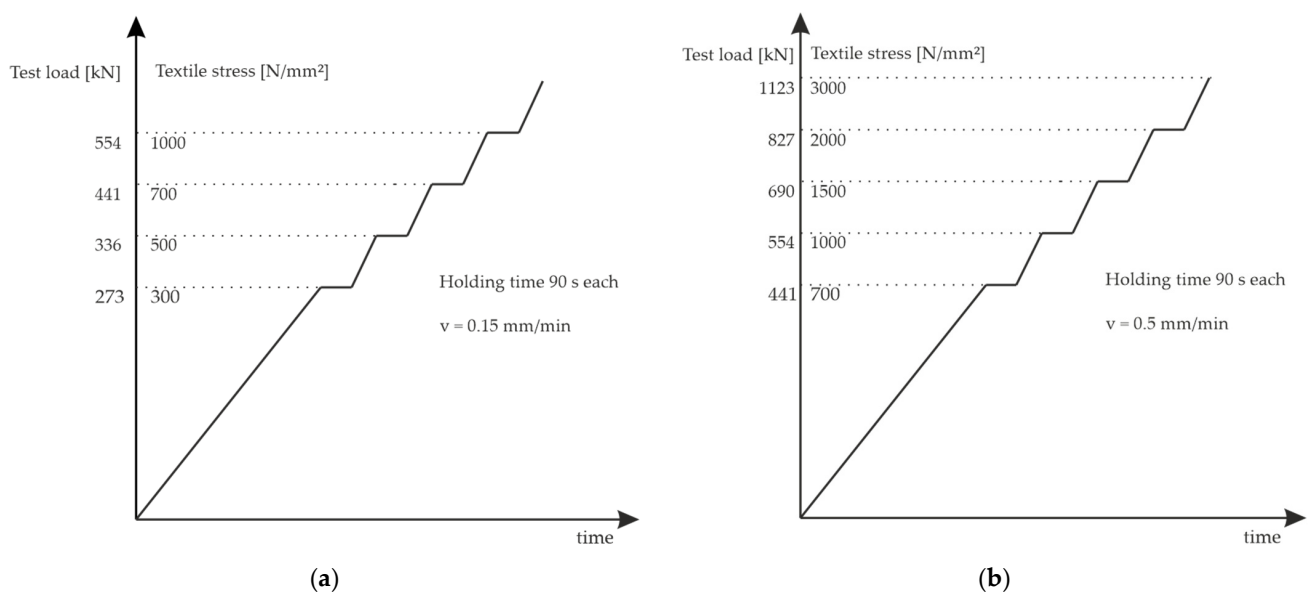


**Figure 19.** Planned load regime: (a) specimen 1; (b) specimen 2. (Graphic: HTWK Leipzig).

## 5.2. Results

### 5.2.1. Results of the Bending Tests

In Figure 20 the moment–deflection curves of the two tested specimens are shown. As it can be seen specimen 2, the one with the doweled ends of the strengthening layer, reaches a much higher load than specimen 1 without anchored ends. The failure loads, resulting moments, and textile stresses in the outer carbon grid at the moment of failure are presented in Table 6.

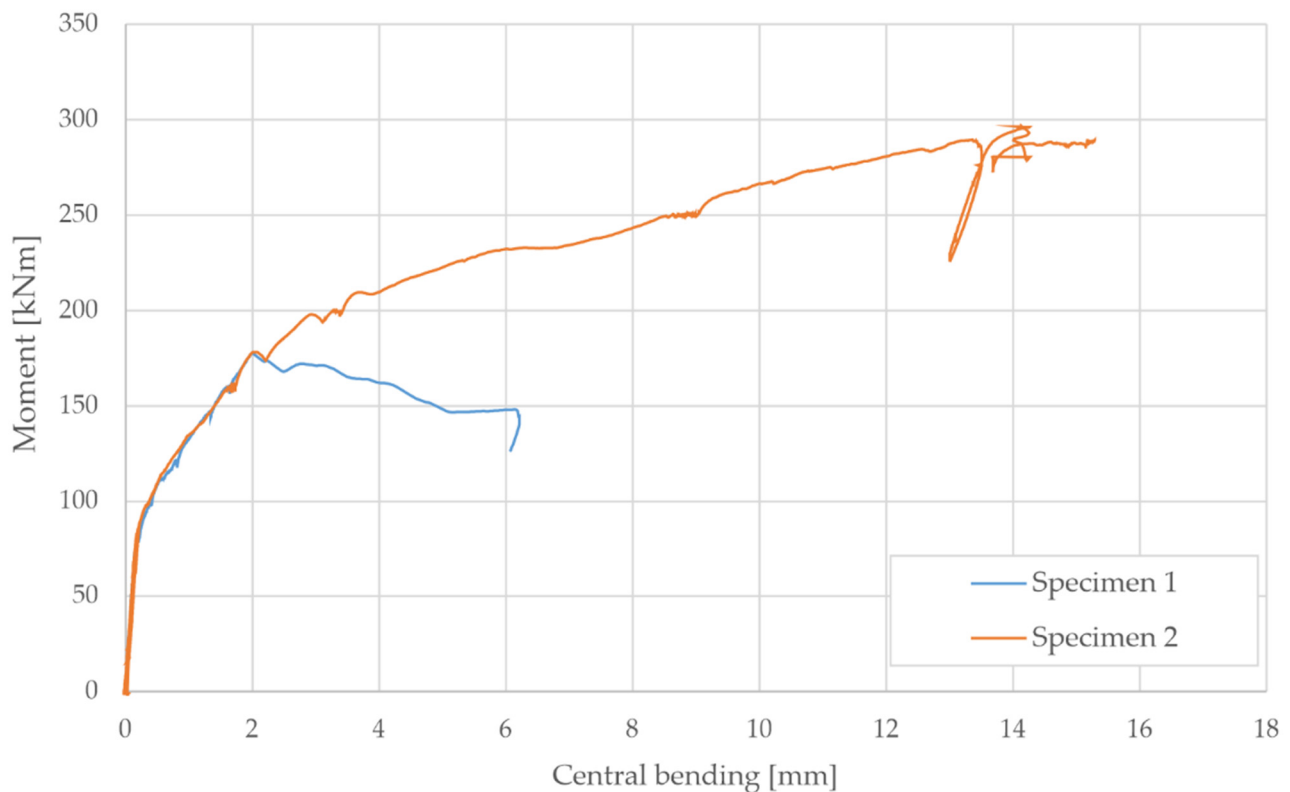


**Figure 20.** Moment-deflection-curves of the two bending tests.

**Table 6.** Results of the bending tests.

Specimen	Failure Load [kN]	Resulting Moment [kNm]	Max. Textile Stress [N/mm <sup>2</sup> ]
1	490	178	778
2	818	296	1965

Even though the failure load could be increased by using dowels for anchoring the ends of the strengthening layer, the maximum textile stress of specimen 2 was below the characteristic tensile strength of the used carbon grid (see Section 2.3.2). Therefore, specimen 1 as well as specimen 2 failed due to concrete cover separation (see Figure 21) and the strengthening layer could not be taken full advantage of.



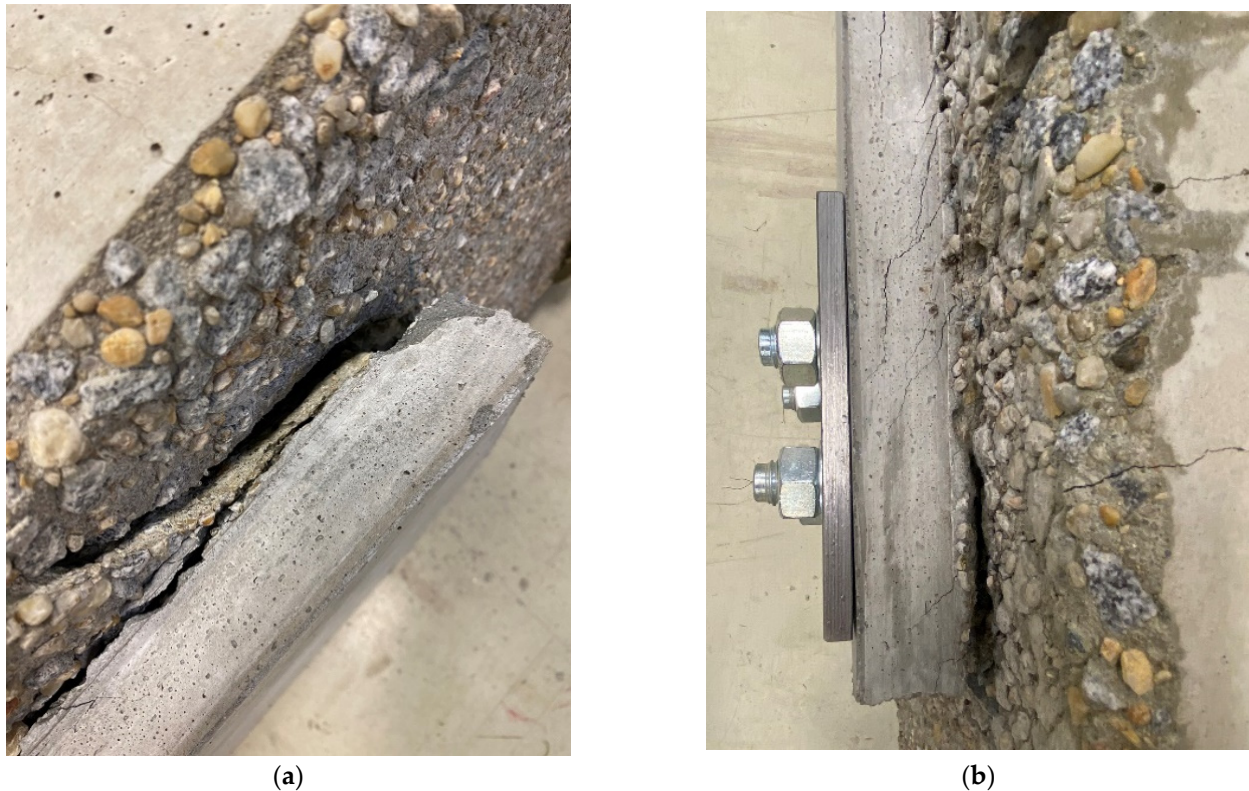


**Figure 21.** Concrete cover separation: (a) specimen 1; (b) specimen 2. (Photo: CARBOCON GMBH).

#### 5.2.2. Dowel Loads

During testing specimen 2, the strain  $\varepsilon_{\text{dowel}}$  of some of the dowels was recorded. With the help of the E-modulus  $E_{\text{dowel}}$  of the dowels, the dowel-forces could be calculated with Equation (1):

$$F_{\text{dowel}} = \sigma_{\text{dowel}} \cdot A_{\text{dowel}} = E_{\text{dowel}} \cdot \varepsilon_{\text{dowel}} \cdot A_{\text{dowel}} \quad (1)$$

As the exact E-modulus of the dowels is unknown, a typical E-modulus for steel of  $210,000 \text{ N/mm}^2$  was assumed. In Figure 22, the dowel loads are contrasted with the moment-deflection curve of specimen 2. It was planned to record the strains of two dowels of each end of the strengthening layer, however the measuring failed for one dowel. Therefore, only three dowels were recorded: two on the left and one on the right side of the beam. It can be seen that, up to a moment of approximately  $150 \text{ kNm}$ , no load is introduced into the dowels. After that, the dowels on the left side of the strengthening layer (green lines) receive tension forces and the dowel on the right side (purple line) received a compression force. It is assumed that at the point when the dowels receive load, the specimen would have failed due to concrete cover separation without dowels.



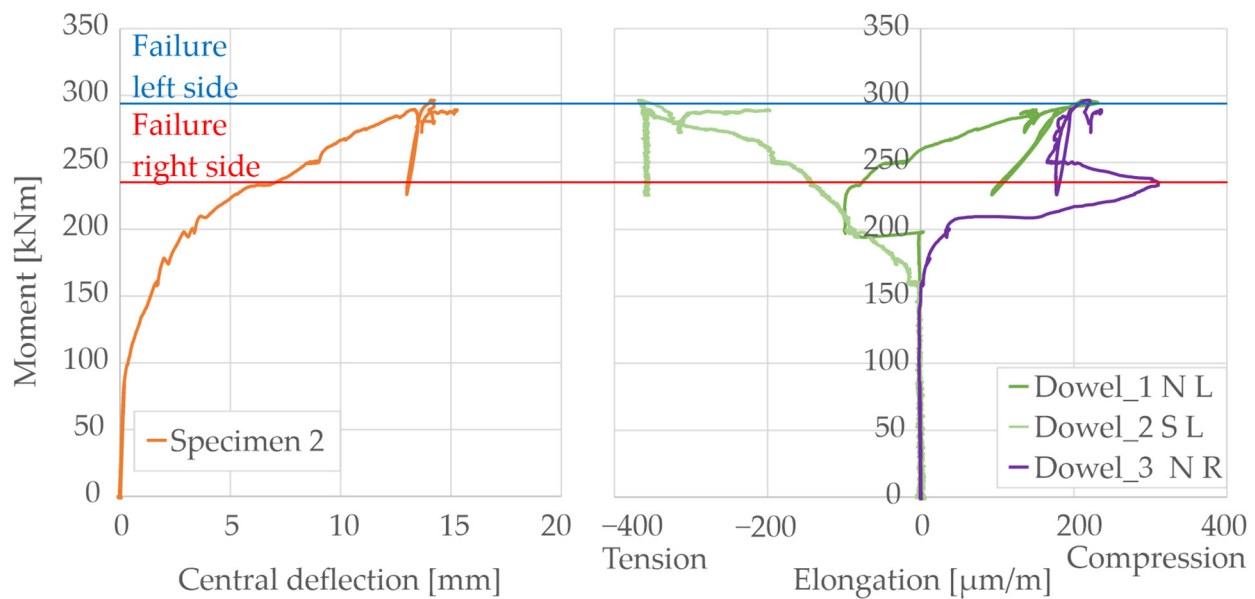


**Figure 22.** Measured dowel loads.

At a moment of approximately 232 kNm, a failure of the right side of the strengthening layer was detected. In Figure 22, it can be seen that at the same point, the measured dowel force decreases (purple line). So, the failure of the anchored end of the strengthening layer could be recorded within the dowels. The maximum load measured in the dowel was 23 kN (compression). In Figure 23, the ends of the strengthening layer are shown right after failure of the right side of specimen 2. Here, it can also be seen why a compression force was recorded in the dowel on the right side: the debonding of the strengthening layer started at the end of the strengthening and reaches to the center of the dowel group. In this point, a moment may be imagined, resulting in tension forces in the dowels reaching through the interfacial debonding crack and compression forces in the dowels on the other side of the dowel group.



**Figure 23.** Anchored ends of the strengthening layer at the moment of failure of the right side: (a) left side; (b) right side. (Photos: CARBOCON GMBH).

Even though the anchoring of the right side of the strengthening layer failed, the loading of specimen 2 could be increased up to a moment of 294 kNm. However, it has to be noted that the failed right end of the strengthening layer was supported after failure and thus further debonding was prevented. In Figure 22, a failure of the anchoring of the

left side of the strengthening layer (green lines) can be recognized at the maximum reached moment of 294 kNm. The maximum recorded load in the dowel on this side was  $-27.3$  kN (tension). Afterwards, the test was stopped, as no load increase was possible anymore.

### 5.2.3. Recalculation of the Experiments

After finishing the tests, the final crack state of the specimens was documented. It is shown for each of the specimens in Figures 24 and 25. Additionally, the strut-and-tie model, presented in Section 4.1, is supplemented. One can see that the strut-and-tie-model fits very well with the final crack states of both specimens. The slope of the compression struts mostly matches the slope of the cracks of the specimens.

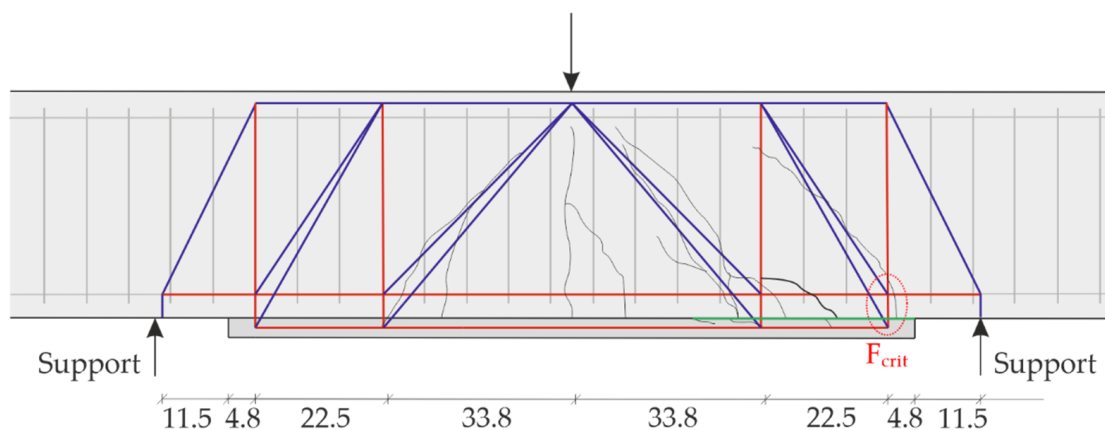


**Figure 24.** Final crack state and strut-and-tie-model for specimen 1. (Graphic: CARBOCON GMBH).

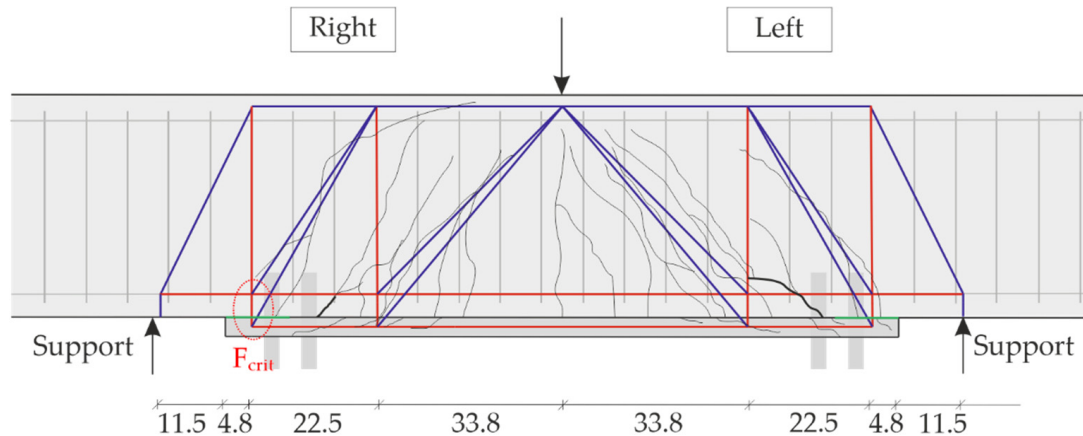


**Figure 25.** Final crack state and strut-and-tie-model for specimen 2. (Graphic: CARBOCON GMBH).

In Figure 26, the calculated loads of the most relevant struts at the moment of failure of both specimens are shown. One may assume that the difference of forces  $\Delta F$  in the critical tensile struts  $F_{crit}$  between both specimens is carried by the dowels. As the difference is  $\Delta F = 322 \text{ kN} - 154 \text{ kN} = 168 \text{ kN}$  and there are four dowels per critical tensile strut, each dowel should carry a load of  $F_{dowel} = 168 \text{ kN} / 4 = 42 \text{ kN}$ . However, the measured dowel tensile loads in Figure 22 show a maximum carried load of 27.3 kN. Possible causes, explaining that difference of  $42 \text{ kN} - 27.3 \text{ kN} = 14.7 \text{ kN}$  between the calculated and measured dowel loads are discussed in the following section.

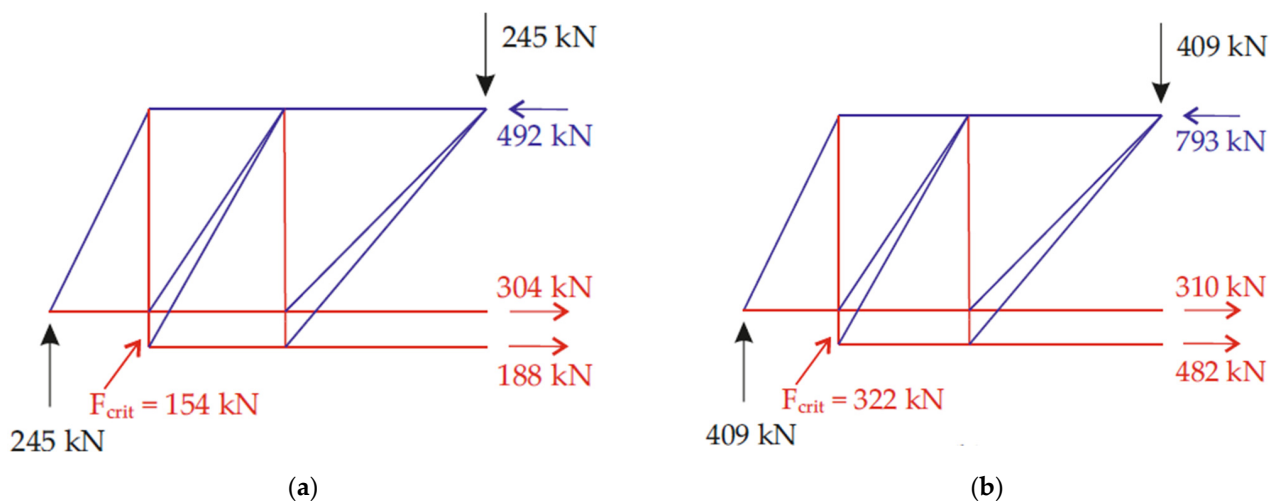


**Figure 26.** Tensile and compression loads of the specimens when reaching the maximum load: (a) specimen 1; (b) specimen 2. (Graphic: CARBOCON GMBH).

### 5.3. Discussion of Possible Causes for the Difference between Measured and Calculated Dowel Loads

#### 5.3.1. Overview

Several possible causes for the difference between the measured and calculated dowel loads, described in the previous section, are listed below:

- As each testing configuration was only tested on one specimen, the obtained results cannot be assumed as mean values. Therefore, differences due to scattering of the testing results may occur.
- When calculating  $F_{crit}$  in the strut-and-tie-model, centric tension in the dowels is assumed. However, due to the failure of the bonding area between carbon reinforced concrete and reinforced concrete, bending of the dowels instead of centric tension may also be possible.
- The bores for the strain gauges inside the dowels may not have been located exactly in the center of each dowel. In the case of the dowels receiving little bending, the mean strain of the dowel may be over- or underestimated, and thus also the calculated forces.
- Errors of the measurement of strain inside the dowels may have occurred.
- The location of the resulting force of the dowel group did not match the location of the critical tensile strut. This deviation may lead to differences between the measured and calculated dowel forces.
- As the measured dowel forces were calculated from the measured strains, the difference between the measured and calculated dowel forces may result from assuming a wrong E-modulus for the dowels.
- As the slope of the compression struts of the assumed strut-and-tie-model does not always match the real slope of the cracks of the specimens (especially specimen 2), it may be possible that the assumed strut-and-tie model is incorrect.
- When installing the dowels, they were prestressed by applying a tightening torque of 200 Nm. However, the measuring of the strain of the dowels was only started after prestressing. Therefore, the force inside the dowels due to their prestressing may have to be added to the measured dowel forces.

Each of the previously presented causes may be the relevant for the difference between the measured and the calculated dowel forces. However, the causes 1–5 cannot be checked anymore for several reasons. Causes 6–8 are discussed in the following sections.

#### 5.3.2. Discussion of the E-Modulus

For the calculation of the dowel forces, a typical E-modulus for steel of  $E_{dowel} = 210,000 \text{ N/mm}^2$  was assumed for the dowels. In rearranging Equation (1) and setting the calculated dowel force of

42 kN as  $F_{\text{dowel}}$ , one can calculate the necessary E-modulus  $E_{\text{dowel}}$  for reaching a match between the calculated and measured dowel forces. For this, the measured maximum strain  $\varepsilon_{\text{max,dowel}}$  was used:

$$E_{\text{dowel}} = (F_{\text{dowel}} / A_{\text{dowel}}) / \varepsilon_{\text{max,dowel}} = (42 \text{ kN} / 353 \text{ mm}^2) / 0.369\text{‰} = 322,439 \text{ N/mm}^2 \quad (2)$$

As one can see in Equation (2), a theoretical E-modulus of 322,439 N/mm<sup>2</sup> would have been necessary for reaching a match between the calculated and measured dowel forces. Such a high E-modulus is unrealistic for steel. Therefore, even if the assumed E-modulus of the dowels is not correct, one may not reach the calculated dowel forces in setting another realistic value for the E-modulus. As a result, cause no. 6 from Section 5.3.1. may be eliminated as a reason for the difference between the measured and calculated dowel forces.

### 5.3.3. Discussion of the Strut-and-Tie-Model

The strut-and-tie-model used for calculating the forces in the critical tensile strut contains two vertical tensile struts over the length between the support and the load introduction point. The slope of the compression struts is the result of the arrangement of the tensile struts. However, especially for specimen 2, the slope of some cracks runs much steeper than the slope of the compression strut (Figure 25). Therefore, the strut-and-tie-model was adapted as described in the following. For the adapted strut-and-tie-model three instead of two vertical tensile struts were arranged over the length between the support and the load introduction point (Figure 27). In doing so, the position of the outer tensile strut (the one containing the critical tensile strut) remained the same. The other two tensile struts were arranged nearly equally over the length between the outer tensile strut and the load introduction point, namely so that their position matches the position of the vertical shear reinforcement. Again, the slope of the compression struts results from the position of the tensile struts. As one can see, the slope of the cracks and the one of the compression struts match very well now.

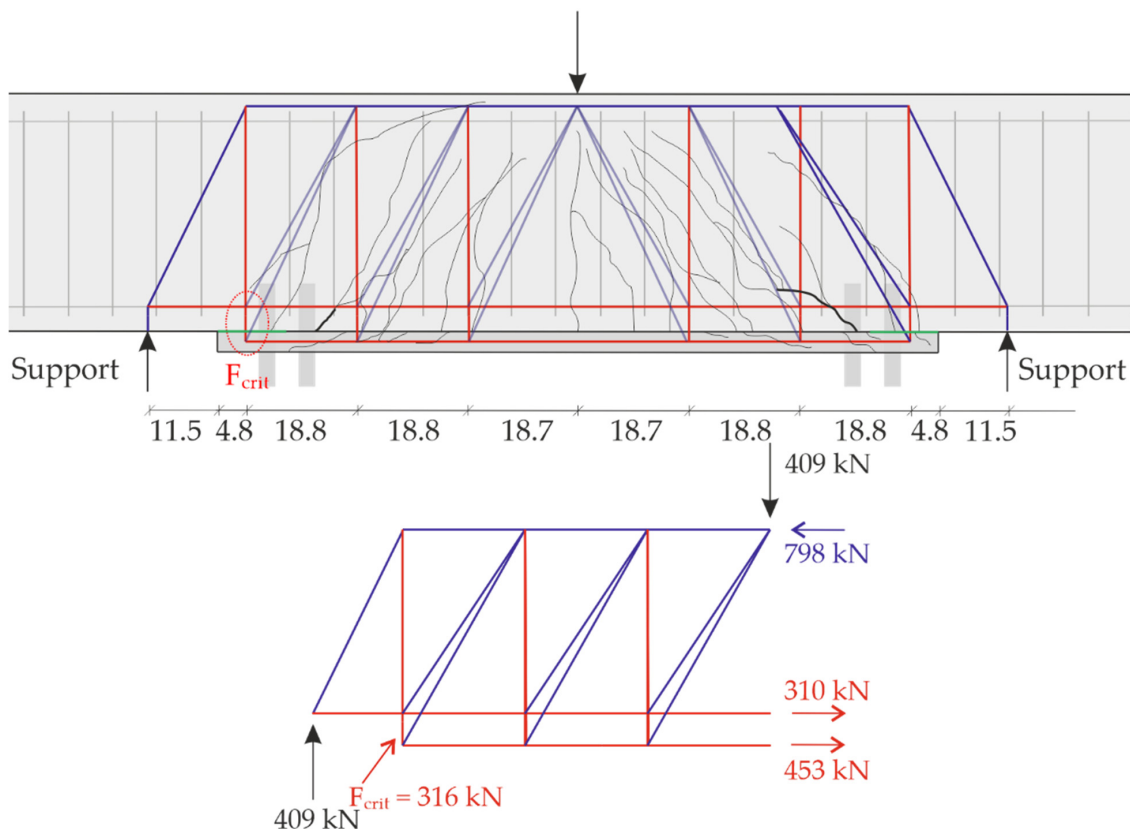


**Figure 27.** Adapted strut-and-tie-model. (Graphic: CARBOCON GMBH).

In Figure 27, the calculated loads in the most important struts of the strut-and-tie-model at the moment of failure of the specimen are presented. The load in the critical tension strut results in 316 kN. For comparison, the force in the critical tension strut before adapting the strut-and-tie-model was 322 kN. Therefore, adapting the strut-and-tie-model does not lead to a significant change of the calculated dowel loads and cause no. 7 from Section 5.3.1. may be eliminated as reason for the difference between the measured and calculated dowel forces, as well.

#### 5.3.4. Discussion of the Prestressing of the Dowels

The last possible cause for the difference between the measured and calculated dowel loads is the not recorded load due to the prestressing of the dowels. They were prestressed by applying a tightening torque of 200 Nm. For calculating the resulting prestressing force  $F_A$  in the dowel, a lot of different parameters have to be taken into account. The calculation is performed with the general equation for the tightening torque  $M_A$ , resulting as the sum of a torque  $M_K$  depending on the friction under the screw head and a torque  $M_G$  depending on the friction along the screw thread (Equation (3) and Figure 28). For calculating the resulting prestressing force  $F_M$ , Equation (3) was rearranged (Equation (4)):

$$M_A = M_K + M_G = F_M \cdot D_{KM} / 2 \cdot \mu_K + F_M \cdot d_2 / 2 \cdot \tan(\varphi + \rho') \quad (3)$$

$$F_M = M_A / D_{KM} / 2 \cdot \mu_K + d_2 / 2 \cdot \tan(\varphi + \rho') \quad (4)$$

with  $\tan \rho' = \mu_G / \cos \alpha / 2$

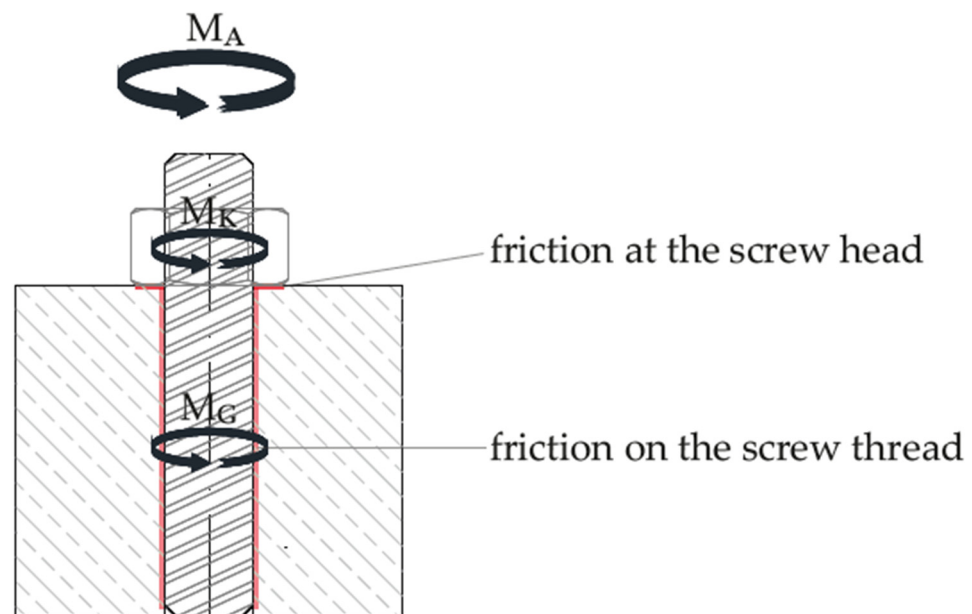


Figure 28. Parts of the tightening torque. (Graphic: CARBOCON GMBH).

For solving Equation (4), the necessary parameters were defined as follows:

- $M_A$ : the tightening torque was set to 200 Nm;
- $D_{KM}$ : the mean diameter of the screw head was set to 37.78 mm, according to [49] for M24 screws;
- $\mu_K$ : the coefficient of friction under the screw head was set to 0.125, according to recommendations for electrogalvanized surfaces (e.g., [50]);
- $d_2$ : the pitch diameter of the screw threads was set to 22.051 mm, according to [51] for M24 screws;
- $\varphi$ : the pitch angle of the screw threads was set to  $2.48^\circ$ , according to [51] for M24 screws;
- $\mu_G$ : the coefficient of friction of the screw threads was set to 0.14, according to recommendations for metric ISO-threads in accordance with [51] (e.g., [52]);



- $\alpha$ : the flank angle of the screw threads was set to  $60^\circ$ , according to [51] for M24 screws.

Solving Equation (4) with the assumptions previously made results in a prestressing force of one single dowel of 38.43 kN. Comparing this result with the difference of 14.7 kN between the calculated and measured dowel load in Section 5.2.3., one may assume that this difference might result from the not recorded prestressing of the dowel. However, the calculated prestressing force is much higher than the difference between the measured and calculated dowel force. In calculating the prestressing force, a lot of assumptions were made, and the calculated prestressing force might rather be understood as an estimation. Nevertheless, the calculation of the prestressing force proves that it might be possible to reach forces in the dowel, which might explain the difference between the measured and calculated dowel loads in the experiments. In order to be able to calculate the dowel loads more accurately in the future, further investigations must be carried out.

## 6. Conclusions

CRC has a high potential to save resources compared to other strengthening methods. However, when strengthening structures with CRC, in some cases, a concrete cover separation is detected as the critical failure mode.

For the prediction of this kind of failure on the one hand, a strut-and-tie-model is presented in this paper. With the help of this, it is possible to determine a critical tensile force leading to failure. To eliminate the problem of concrete cover separation on the other hand, several possible solutions were suggested. One of them is the use of dowels at the ends of the strengthening layer to introduce higher forces into the existing concrete structure. This solution was tested in preliminary experimental investigations and presented in this paper.

For this, two reinforced concrete beams with a CRC strengthening layer were tested in three-point bending tests. The ends of the strengthening layer of one of the beams were doweled whereas the other specimen was tested without any additional anchoring of the strengthening layer. It was shown that the doweled specimen reached a much higher load than the other one. However, even the dowelled specimen still failed due to concrete cover separation. Additionally, the tests have shown that the developed strut-and-tie-model fits very well with the final crack states of both specimens.

With the help of the tests, it was possible to show that anchoring the ends of the strengthening layer with dowels is one way of improving the load-bearing capacity of a CRC strengthening layer. Besides the use of dowels, additional ideas to improve the load-bearing capacity of the bonding area between CRC and RC will be the subject of further investigations.

**Author Contributions:** Conceptualization, J.W., E.S., A.S. and L.N.; methodology, J.W., C.W., E.S., A.S., L.N. and M.C.; software, D.E. and L.N.; validation, E.S. and D.E.; formal analysis, J.W., C.W. and L.N.; investigation, J.W., C.W. and L.N.; resources, C.W.; data curation, C.W. and D.E.; writing—original draft preparation, J.W., A.S., E.S. and C.W.; writing—review and editing, J.W., E.S., A.S. and C.W.; visualization, J.W., C.W. and E.S.; supervision, E.S. and D.E.; project administration, J.W. and A.S.; funding acquisition, A.S., E.S., D.E. and L.N. All authors have read and agreed to the published version of the manuscript.

**Funding:** This research was funded by AiF Projekt GmbH, grant number KK5242601CD1.

**Institutional Review Board Statement:** Not applicable.

**Informed Consent Statement:** Not applicable.

**Data Availability Statement:** Not applicable.

**Acknowledgments:** The authors would like to thank the colleagues in the laboratory of HTWK Leipzig, where the specimens were tested.

**Conflicts of Interest:** The authors declare no conflict of interest. The funders had no role in the design of the study; in the collection, analyses, or interpretation of data; in the writing of the manuscript, or in the decision to publish the results.

## References

- Weidner, S.; Mrzigod, A.; Bechmann, R.; Sobek, W. Graue Emissionen im Bauwesen—Bestandsaufnahme und Optimierungsstrategien. *Beton-Und Stahlbetonbau* **2021**, *116*, 969–977. [\[CrossRef\]](#)
- Meier, U. Strengthening of structures using carbon fibre/epoxy composites. *Constr. Build. Mater.* **1995**, *9*, 341–351. [\[CrossRef\]](#)
- Chajes, M.J.; Thomson, T.A.; Januszka, T.F.; Finch, W.W. Flexural strengthening of concrete beams using externally bonded composite materials. *Constr. Build. Mater.* **1994**, *8*, 191–201. [\[CrossRef\]](#)
- M'Bazaa, I.; Missihoun, M.; Labossiere, P. Strengthening of Reinforced Concrete Beams with CFRP Sheets. In Proceedings of the ICCI'96, Proceedings of the Fiber Composites in Infrastructure (ICCI'96), Tuscon, AZ, USA, 15–17 January 1996; pp. 746–759.
- Bakis, C.E.; Bank, L.C.; Brown, V.; Cosenza, E.; Davalos, J.F.; Lesko, J.J.; Machida, A.; Rizkalla, S.H.; Triantafillou, T.C. Fiber-Reinforced Polymer Composites for Construction—State-of-the-Art Review. *J. Compos. Constr.* **2002**, *6*, 73–87. [\[CrossRef\]](#)
- Mostofinejad, D.; Shameli, S.M. Externally bonded reinforcement in grooves (EBRIG) technique to postpone debonding of FRP sheets in strengthened concrete beams. *Constr. Build. Mater.* **2013**, *38*, 751–758. [\[CrossRef\]](#)
- Andrä, H.P.; Maier, M. Post-Strengthening of RC Structures with Externally Bonded Prestressed CFRP Strips. In Proceedings of the 16th IABSE Congress, Luzern, Switzerland, 18 September 2000; pp. 18–21, 1507–1514.
- Derkowski, W. The First National Application of Pre-Tensioned Composite Strips to Strengthen the Hall Structure. *Czas. Tech.* **2007**, *4*, 265–270.
- Zdanowicz, Ł.; Seręga, S.; Tekieli, M.; Kwiecień, A. Polymer Flexible Joint as a Repair Method of Concrete Elements: Flexural Testing and Numerical Analysis. *Materials* **2020**, *13*, 5732. [\[CrossRef\]](#)
- Lye, H.L.; Mohammed, B.S.; Liew, M.; Wahab, M.; Al-Fakih, A. Bond behaviour of CFRP-strengthened ECC using Response Surface Methodology (RSM). *Case Stud. Constr. Mater.* **2019**, *12*, e00327. [\[CrossRef\]](#)
- Rahim, N.I.; Mohammed, B.S.; Al-Fakih, A.; Wahab, M.M.A.; Liew, M.S.; Anwar, A.; Amran, Y.H.M. Strengthening the Structural Behavior of Web Openings in RC Deep Beam Using CFRP. *Materials* **2020**, *13*, 2804. [\[CrossRef\]](#)
- Müller, E.; Schmidt, A.; Schumann, A.; May, S.; Curbach, M. Biegeverstärkung mit Carbonbeton. *Beton-und Stahlbetonbau* **2020**, *115*, 758–767. [\[CrossRef\]](#)
- Schumann, A.; May, S.; Hoinka, J. Paradigmenwechsel im Bauwesen—Gerade richtig oder schon zu spät? Nachhaltiges Bauen im Bestand mit Carbonbeton. *Ernst & Sohn Special, Nachhaltiges Bauen* **2021**, 13–15.
- Scheerer, S.; Schladitz, F.; Curbach, M. Textile Reinforced Concrete—From the Idea to a High Performance Material. In Proceedings of the FERRO-11 International Symposium on Ferrocement and 3rd ICTRC International Conference on Textile Reinforced Concrete, Aachen, Germany, 7–10 June 2015; Hrsg. Brameshuber, W., Ed.; RILEM Publications S.A.R.L.: Bagneux, France, 2015; pp. 15–33.
- Scheerer, S.; Zobel, R.; Müller, E.; Senckpiel-Peters, T.; Schmidt, A.; Curbach, M. Flexural Strengthening of RC Structures with TRC—Experimental Observations, Design Approach and Application. *Appl. Sci.* **2019**, *9*, 1322. [\[CrossRef\]](#)
- Brückner, A.; Ortlepp, R.; Curbach, M. Anchoring of shear strengthening for T-beams made of textile reinforced concrete (TRC). *Mater. Struct.* **2007**, *41*, 407–418. [\[CrossRef\]](#)
- Weiland, S.; Ortlepp, R.; Brückner, A.; Curbach, M. Strengthening of RC-Structures with Textile Reinforced Concrete (TRC). *Thin Fiber Text. Reinf. Cem. Syst.* **2007**, *244*, 157–172.
- Triantafillou, T. Shear Strengthening of Reinforced Concrete Beams Using Epoxy-Bonded FRP Composites. *ACI Struct. J.* **1998**, *95*, 107–115.
- Bergmann, S.; May, S.; Hegger, J.; Curbach, M. Shear strengthening of reinforced concrete T-beams using carbon reinforced concrete. *Chic. ACI* **2020**, *345*, 169–184.
- Bergmann, S.; May, S. Shear Strengthening of RC T-Beams with CRC. In Proceedings of the Tagungsband der 12. Carbon- und Textilbetontage, Dresden, Germany, 22–23 September 2020; pp. 38–41.
- Escrig, C.; Gil, L.; Bernat-Maso, E.; Puigvert, F. Experimental and analytical study of reinforced concrete beams shear strengthened with different types of textile-reinforced mortar. *Constr. Build. Mater.* **2015**, *83*, 248–260. [\[CrossRef\]](#)
- Schumann, A.; Schöffel, J.; May, S.; Schladitz, F.; Curbach, M. Ressourceneinsparung mit Carbonbeton—Am Beispiel der Verstärkung der Hyparschale in Magdeburg. In *Nachhaltigkeit, Ressourceneffizienz und Klimaschutz, Konstruktive Lösungen für das Planen und Bauen—Aktueller Stand der Technik*; Hrsg. Hauke, B., Institut Bauen und Umwelt e.V., DGNB e.V., Eds.; Ernst & Sohn: Berlin, Germany, 2021.
- Schumann, A.; May, S.; Bochmann, J. Zu neuer Leistungsfähigkeit. *B + B Bau. Im Bestand* **2021**, *1*, 20–25.
- Jesse, F.; Curbach, M. Verstärken mit Carbonbeton. In *BetonKalender 2010—Brücken, Betonbau im Wasser*; Hrsg. Fingerloos, F., Wörner, J.-D., Eds.; Ernst und Sohn: Berlin, Germany, 2010; pp. 457–565.
- Curbach, M.; May, S.; Müller, E.; Schumann, A.; Schütze, E.; Wagner, J. Verstärken mit Carbonbeton. In *Beton-Kalender 2022—Nachhaltigkeit, Digitalisierung, Instandhaltung*; Hrsg. Bergmeister, K., Fingerloos, F., Wörner, J.-D., Eds.; Ernst und Sohn: Berlin, Germany, 2021; pp. 761–804.
- Schumann, A.; Schladitz, F.; May, S.; Scheerer, S. Carbonbeton in der Denkmalsanierung. *Denkmalsanierung* **2020**, *2021*, 2–3.
- Riegelmann, P.; May, S.; Schumann, A. Das Potential von Carbonbeton für den Brückenbestand—das ist heute schon möglich! In *Tagungsband zum 30. Dresdner Brückenbausymposium (Ergänzungsband 2021)* (Hrsg. Curbach, M.); Institut für Massivbau der TU Dresden: Dresden, Germany, 2021; pp. 79–90.

28. Deutscher Ausschuss für Stahlbeton. (*German Committee for Reinforced Concrete*): *Richtlinie Betonbauteile mit nichtmetallischer Bewehrungen*; Draft; Deutscher Ausschuss für Stahlbeton: Berlin, Germany, 2022.
29. Z-31.10-182; Verfahren zur Verstärkung von Stahlbeton mit TUDALIT (Textilbewehrter Beton). abZ, DIBt: Berlin, Germany, 2016.
30. Z-31.10-182; CARBOrefit-Verfahren zur Verstärkung von Stahlbeton mit Carbonbeton. abZ, DIBt: Berlin, Germany, 2021.
31. EN 196-1:2005; DIN EN 196-1 (2005-05): *Methods of Testing Cement-Part 1: Determination of Strength*. German Version. 2005. Available online: <https://standards.iteh.ai/catalog/standards/cen/211ff288-f8ea-4d1d-b62c-967e4d285f17/en-196-1-2005> (accessed on 9 April 2022).
32. Erhard, E.; Weiland, S.; Lorenz, E.; Schladitz, F.; Beckmann, B.; Curbach, M. Anwendungsbeispiele für Textilbetonverstärkung: Instandsetzung und Verstärkung bestehender Tragwerke mit Textilbeton. *Beton-und Stahlbetonbau* **2015**, *110*, 74–82. [CrossRef]
33. Al-Jamous, A.; Uhlig, K. Sanierung der historischen Betonbogenbrücke in Naila. *Tag. Zum* **2017**, *27*, 71–78.
34. Rempel, S.; Erhard, E.; Schmidt, H.-G.; Will, N. Die Sanierung des Mariendomdaches in Neviges mit carbonbewehrtem Spritzmörtel. *Beton-Und Stahlbetonbau* **2018**, *113*, 543–550. [CrossRef]
35. Weiland, S.; Schladitz, F.; Schütze, E.; Timmers, R.; Curbach, M. Rissinstandsetzung eines Zuckersilos. *Bautechnik* **2013**, *90*, 498–504. [CrossRef]
36. Feix, J.; Hansl, M. Pilotanwendungen von Textilbeton für Verstärkungen im Brückenbau. In *Tagungsband zum 25. Dresdner Brückenbausymposium—Planung, Bauausführung, Instandsetzung und Ertüchtigung von Brücken*; Hrsg. Curbach, M., Ed.; Institut für Massivbau der TU Dresden: Dresden, Germany, 2015; pp. 99–110.
37. Schladitz, F.; Schumann, A.; May, S.; Curbach, M. Carbonbetonbau im Brückenbau. *Zeitschrift des Vereins der Straßenbau-und Verkehrsingenieure im Freistaat Sachsen e.V.* **2020**, 34–37.
38. Steinbock, O.; Giese, N.-J.; Curbach, M. Probelastung einer mit Carbonbeton verstärkten Plattenbrücke. In *Tagungsband zum 11. Symposium Experimentelle Untersuchungen von Baukonstruktionen*; Hrsg. Curbach, M., Marx, S., Scheerer, S., Hampel, T., Eds.; Institut für Massivbau der TU Dresden: Dresden, Germany, 8 March 2021; pp. 118–129.
39. Adam, V.; Bielak, J.; Will, N.; Hegger, D.J. Experimentelle Untersuchungen zur Verstärkung von Brückenfahrbahnplatten mit Textilbeton. *Beton-und Stahlbetonbau* **2020**, *115*, 952–961. [CrossRef]
40. Büttner, T. SMART-DECK: Vom Konzept zum Demonstrator. *Bautechnik* **2019**, *97*, 48–56. [CrossRef]
41. Hentschel, M.; Schumann, A.; Ulrich, H.; Jentzsch, S. Sanierung der Hyparschale Magdeburg. *Bautechnik* **2018**, *96*, 25–30. [CrossRef]
42. Riegelmann, P.; Schumann, A.; May, S.; Bochmann, J.; Garibaldi, M.P.; Curbach, M. Muther's shell structures in Germany—A solution to avoid demolition. *Proc. Inst. Civ. Eng.-Eng. Hist. Herit.* **2020**, *174*, 124–132. [CrossRef]
43. Schumann, A.; Hentschel, M.; Zobel, R.; Curbach, M. Strengthening of the Hypar Shell in Magdeburg with Carbon Reinforced Concrete-Design and Calculations. In *Proceedings of the IASS Annual Symposium 2019—Structural Membranes*, Barcelona, Spain, 7–10 October 2019; pp. 855–862.
44. Steinbock, O.; Pelke, E.; Ost, O. Carbonbeton—Eine neue Verstärkungsmethode für Massivbrücken—Teil 1: Grundlagen und Hintergründe zum Pilotprojekt “Brücken über die Nidda im Zuge der BAB A 648”. *Beton-und Stahlbetonbau* **2021**, *116*, 101–108. [CrossRef]
45. Steinbock, O.; Bösch, T.; Schumann, A. Carbonbeton—Eine neue Verstärkungsmethode für Massivbrücken—Teil 2: Carbonbeton im Brückenbau und Informationen zur Zustimmung im Einzelfall für das Pilotprojekt “Brücken über die Nidda im Zuge der BAB A 648”. *Beton-und Stahlbetonbau* **2021**, *116*, 109–117. [CrossRef]
46. Steinbock, O.; Teworte, F.; Neis, B. Carbonbeton—Eine neue Verstärkungsmethode für Massivbrücken—Teil 3: Planung und Umsetzung der Verstärkungsmaßnahme mit Carbonbeton am Pilotprojekt „Brücken über die Nidda im Zuge der BAB A 648“. *Beton-und Stahlbetonbau* **2021**, *116*, 118–126. [CrossRef]
47. Finckh, W. Einfluss Bauteilspezifischer Effekte auf die Bemessung von mit CFK-Lamellen Verstärkten Stahlbetonbauteilen. Ph.D. Thesis, Technische Universität München, Lehrstuhl für Massivbau, München, Italy, 2012.
48. ETA-99/0011; Würth Fixanker W-FAZ und W-FAZ-IG—Mechanische Dübel zur Verwendung im Beton. DIBt: Berlin, Germany, 2018.
49. DIN 7990: 2017-08; Sechskantschrauben mit Sechskantmutter für Stahlkonstruktionen. Beuth: Berlin, Germany, 2017.
50. Available online: <https://www.schrauben-frank.de/technische-informationen/mechanische-eigenschaften/anziehen-v.-schrauben-und-reibwerte/> (accessed on 15 March 2022).
51. DIN 13-1:1999-11; Metrisches ISO-Gewinde Allgemeiner Anwendung—Teil 1: Nennmaße für Regelgewinde; Gewinde-Nenn Durchmesser von 1mm bis 68 mm. Beuth: Berlin, Germany, 1999.
52. Available online: [https://media.wuerth.com/stmedia/shop/masterpages0000/LANG\\_de/09146.pdf](https://media.wuerth.com/stmedia/shop/masterpages0000/LANG_de/09146.pdf) (accessed on 15 March 2022).